Summer 7-24-2023

Signal Classification Based on Analog Computing Using MEMS Network

Mohammad Okour
University of Nebraska-Lincoln

SIGNAL CLASSIFICATION BASED ON ANALOG COMPUTING USING MEMS NETWORK

by

Mohammad J. Okour

A THESIS

Presented to the Faculty of

The Graduate College at the University of Nebraska

In Partial Fulfillment of Requirements

For the Degree of Master of Science

Major: Architectural Engineering

Under the Supervision of Professor Fadi Alsaleem

Lincoln, Nebraska

July 2023

SIGNAL CLASSIFICATION BASED ON ANALOG COMPUTING USING MEMS NETWORK

Mohammad J. Okour, M.S

University of Nebraska, 2023

Adviser: Fadi Alsaleem

The rising complexity of machine learning algorithms and Artificial Intelligence in many applications, such as smart building, has prompted the development of alternate computing options. Because of their compact size, low power consumption, and diverse functionality, microelectromechanical systems (MEMS) have emerged as a possible candidate. This thesis focuses on using MEMS networks as computing units to classify a simple signal classification task using neural network methodology. The study intends to show the potential of using MEMS as an analog computing unit by discussing the advantage of the bi-stability pull-in behavior and hysteresis to create an accurate classifier of these waveforms. Modeling and simulation are being conducted to assess the MEMS-based computer units performance. The results reveal that the proposed methodology performs the required classification without requiring a digital computer. Furthermore, This study adds to the field of analog computing with MEMS by providing insights into the feasibility and potential of using MEMS networks for more complex classification tasks such as those related to smart building applications

ACKNOWLEDGMENTS

I wish to extend my deepest gratitude to the following people who were always there to support and encourage me throughout this journey.

I would like to thank my advisor, Professor Fadi Alsaleem, for his help and mentorship throughout my graduate studies, Professor Moe Alahmad, and Professor Milad Roohi who are serving on my committee.

Also, I would like to acknowledge the funding support from an IARPA grant led by GE research. The team Dr. David Lin has instrumental feedback to accomplish the work.

Finally, I would never be able to express my profound gratitude towards my parents, family, friends, and wife and child for their support.

Table of Contents

List of Figures

List of Tables

CHAPTER 1

INTRODUCTION AND BACKGROUND

1.1 Motivation

The need for small, energy-efficient solutions has grown significantly in computing. Although digital computing has been the dominating paradigm, its size and power consumption drawbacks have led to the investigation of alternate strategies. With its inherent benefits, analog computing has emerged as a possible answer to these problems. Analog computing has distinct advantages over digital computing, including energy efficiency, real-time processing, and the opportunity for compact implementations. Microelectromechanical systems (MEMS) offer an implementation platform for analog computing [20]. As a demonstration, this research focuses on the advantages of analog computing for signal classification tasks by employing MEMS properties, such as hysteresis and bi-stability pull-in, because of their electrostatic actuation. Electrostatic actuation results from the interaction of electric charges between the fixed electrode and the beam in MEMS. This force has enabled accurate, precise microscale actuation, sensing, and control [34-37]. Traditional waveform classification techniques rely on computationally intensive digital signal processing algorithms or specialized hardware, which uses much energy and space. The potential for low power consumption and the small size of MEMS-based analog computing units, in contrast, addresses the drawbacks of the

digital method. MEMS devices are exceptional options for practical and compact waveform categorization due to their unique characteristics, including their capacity to execute analog computations and use hysteresis.

This thesis aims to contribute to energy-efficient and portable computing solutions by adopting analog computing concepts using MEMS devices. The findings of this study have the potential to revolutionize waveform classification and encourage more analog computing research in various fields. In addition to providing a superior method for classifying triangle and square waveforms, MEMS-based analog computing also permits improvements in challenging computational tasks, ultimately spurs the creation of effective and portable computing systems.

1.2 Literature Review

Modern computing has a growing demand for faster processing units that can efficiently handle the increasing complexity of problems in machine learning algorithms and artificial intelligence applications. This demand is expected to continue growing shortly. These fields demand enormous processing power to handle enormous volumes of data and carry out intricate computations in real-time. On the other hand, traditional computer technologies have several significant drawbacks, including high power consumption and scaling restrictions. Researchers have focused on using other technologies, including MEMS, as a viable solution to address these difficulties. MEMS are small-scale devices integrating mechanical and electronic components to perform various activities. Due to

their durability, compact size, and low power consumption [14-16], MEMS are employed extensively as sensors [1-3], actuators [4-6], switches [7], wearable devices [8-10], and computer systems [11-13]. In addition to these applications, they have recently been proposed to be used in applications related to neuromorphic computing systems [31].

The structure and operation of the human brain have served as a source of inspiration for a new approach to computing known as neuromorphic computing. It requires specialized hardware and software systems to imitate how information is processed and stored within the human brain. Utilizing MEMS is one of the most critical aspects of neuromorphic computing. Neuromorphic computers do computation utilizing physical hardware as opposed to a digital circuit. Considering this, electrostatic MEMS devices have shown they can carry out at least two distinct neuromorphic computing approaches. The first is known as normal neural network-based computing (N.N), while the second is known as reservoir computing (R.C) [32-33].

In the N.N. approach, a network of MEMS resonators was proposed first to perform recognizing spoken digits task [18]. In addition to that, a MEMS system with self-oscillators was modeled and simulated. The system demonstrated the capability of auto-associative memory operation with high robustness of pattern retrieval in the presence of nonlinearity, frequency and coupling strength dispersion, and white noise perturbations. However, to ensure that the system's performance is as it should be, a narrow frequency distribution is required, as this will prevent the system from performing as it should not. In addition to this, there will need to be stringent limitations placed on the repeatability of coupling strengths. The findings show that neurocomputing in a physically realistic

network of micromechanical oscillators using a manufacturing process based on silicon can be resistant to noise sources and fabrication [19].

Alternatively, another piece of research presents an original idea for employing MEMS as a computing unit. The theory underpinning the concept is derived from the neuron rate model theory, an essential component of dynamic field theory. This theory is used for modeling of cognition and human behavior. The simulation of the detection and memory capacities of a single rate model neuron is accomplished by using the proposed approach, which uses the nonlinear dynamics of MEMS resonators, in particular, bi-stability and hysteresis [20]. In addition, a modeled simulation of MEMS suggested that continuous time recurrent neural network may serve as a foundation for human actions to be recognized. Hysteresis, in conjunction with pull-in or nonlinear arch geometries, enables tiny MEMS networks to represent the basic features of CTRNNs qualitatively and effectively. In this study, various neuron types were tested in the hidden layer, and the results were compared to those predicted by the long short term memory (LTSM) and CTRNN models. According to the findings, the MEMS-based CTRNN model's average accuracy in classifying five distinct activities is 77.94% compared to the standard CTRNN's 78.48% accuracy [21].

In yet another significant body of work, the categorization of a triangle and square signals was accomplished by using a three-node MEMS network that was mechanically connected. It is just necessary to apply a D.C. bias voltage to operate the network to complete the task. The work consisted mainly of simulation findings, with the classification tasks being effectively completed without using any circuits or other external processing devices [22].

However, using mechanical connections between the MEMS limit the use of this computing unit for other applications. In this thesis, we present electrical connections with adjustable weights. This allows its reconfiguration to fit more than one application.

A different method of neuromorphic computing was introduced in the middle of the 2000s [17]. Reservoir computing, a computational paradigm inspired by the dynamics of physical systems, utilizes the concept of a "reservoir" to perform complex computations. The reservoir, implemented using physical systems such as electronic circuits or optoelectronic devices, exhibits rich and nonlinear dynamics that enable efficient information processing [23,24]. In reservoir computing, the transformed representation from the reservoir is further processed by a linear regression layer. Using a simple linear function, this layer maps the reservoir's state to the desired output. There is a possibility that this method could be used to directly carry out time series analysis [25-27]. Modifying a MEMS RC system utilizing the mutual information criterion proved successful. The findings show that a statistical model with an unimodal aim distribution can prevent chaos. The distribution will maximize the desired outcome's likelihood. Tuning the equilibrium between MEMS reservoir linearity and nonlinearity increases prediction accuracy [28]. This is a consequence of the tuning technique. In addition, MEMS R.C. accelerometers have been devised and constructed with the capacity to do sensing and calculation activities. The design comprises a connected beam responsible for the processing work and an accelerometer MEMS responsible for sensing motion to measure acceleration. Integrated systems are characterized by enhanced speed, lower

power consumption, and reduced size. This is in comparison to discrete modules used for sensing and regulating [29].

Despite the amount of work on MEMS RC, MEMS neural network computing still offers precise control over individual neural network elements, allowing for fine-tuned computations and higher accuracy than MEMS reservoir computing. Its flexibility in architectural design enables the implementation of various neural network models and algorithms, adapting to diverse problem domains. Additionally, MEMS neural network computing excels in parallelism, processing multiple inputs simultaneously for accelerated computations. In contrast, MEMS reservoir computing relies on sequential processing, potentially limiting processing speed.

This thesis aims to investigate the feasibility of using MEMS networks as computing units for categorizing triangle and square waveforms using neural network computing methodology. The neural network approach will use MEMS devices' nonlinear dynamics and hysteresis to imitate rate model neurons' detection and memory capabilities. To evaluate the network's performance in identifying triangle and square waveforms, the research result will be based on simulation, and future work on experimental tests including both fabrication and testing of the network. This is expected to outperform typical digital computing methods in classification accuracy by using the unique features of MEMS. Second, the study emphasizes the benefits of adopting MEMS-based computing units, such as low power consumption, compact size, and parallelism, which can benefit real-time and portable applications. Overall, this research will add to the increasing body of knowledge on analog computing with MEMS and provide insights into the practicality and promise of

using MEMS networks for waveform categorization tasks using neural network methodology.

1.3 Thesis Objectives

This thesis investigates the feasibility and effectiveness of utilizing a MEMS network as a computing unit for classifying triangle and square waveforms. The network parameters will be optimized to ensure reliable and accurate classification. Considerations related to power consumption and scalability will be addressed to ensure the proposed MEMS-based solution's practical viability and applicability. By achieving these objectives, this research aims to contribute to creating new analog computing concept for signal classification techniques, demonstrate the potential of MEMS networks as novel computing units, and provide insights for the development of efficient and compact systems for real-time waveform analysis and recognition in diverse fields such as telecommunications, biomedical engineering, and internet of things (IoT) devices.

1.4 Problem Statement

MEMS have seen remarkable developments in recent years, which has opened up new possibilities for constructing effective computing units. These small devices have extraordinary capabilities, such as low power consumption, a compact design, and a high

integration density. This thesis uses the potential offered by MEMS technology as a computing unit to categorize triangular and square waveforms. Because of the similarities between triangle and square waveforms in terms of amplitude, classifying these two types of waveforms presents a considerable issue. For example, when the amplitude of each of these waveforms is the same, conventional methods, such as employing simple switches, are unable to differentiate between them accurately, Because of this constraint, there is a pressing need for more advanced processing units to identify minor waveform properties to accomplish reliable categorization, as shown in Figure 1.1

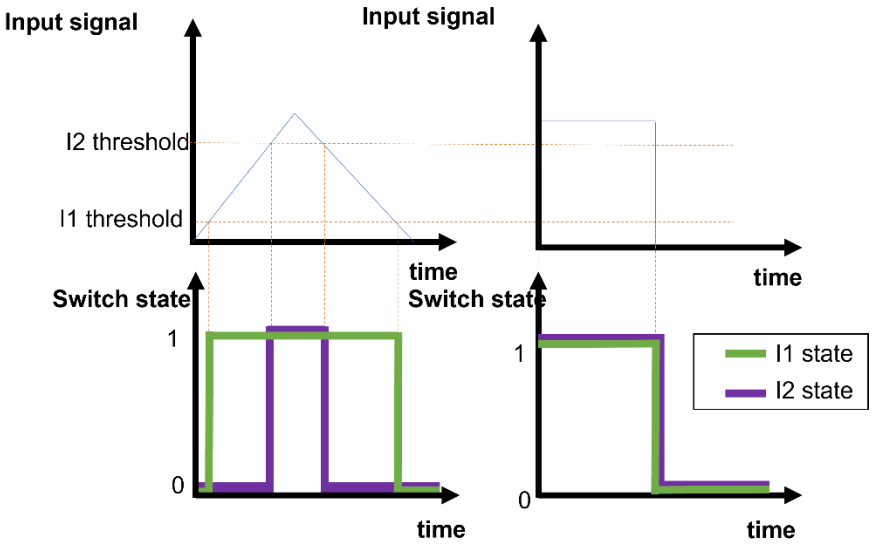

Figure 1.1: Signal classification using switches is not trivial.

A MEMS network is an exciting possibility for a solution in this scenario. Hysteresis is one of the distinctive qualities that MEMS devices show; this property, along with others, can improve waveform classification. The MEMS can have some memory by taking advantage of the hysteresis phenomenon, which makes it possible for the network to distinguish between triangular and square signals even when the amplitudes of the signals

are the same. In MEMS, the hysteresis effect describes the dependence of the device's output on its previous states. Due to the presence of this attribute, the MEMS network can store information regarding the waveform shape and its history. Incorporating this property into the architecture of the network makes it possible to use the MEMS hysteresis as a memory element, which in turn gives the network the ability to differentiate between triangle and square waveforms based on the distinctive temporal characteristics of each waveform.

Utilizing a MEMS network as a computing unit for the classification of triangle and square waveforms offers several benefits compared to more conventional methods. To begin, MEMS devices' inherent analog computation capabilities to make real-time processing possible and lower the computational burden generally associated with digital signal processing algorithms. This enables the devices to reduce the time needed to complete a task. Additionally, MEMS devices are suited for integration into portable and resource-constrained systems because of their small size and low power consumption. This makes MEMS devices an attractive option.

This thesis intends to overcome the complications associated with reliably identifying triangle and square waveforms by investigating the potential of MEMS hysteresis as a memory element within the network. In other words, the thesis will explore the potential of MEMS hysteresis as a memory element. In addition to contributing to waveform classification techniques, the successful development of such a computer unit based on MEMS will demonstrate the usability of MEMS technology in sophisticated signal processing systems.

CHAPTER 2

ELECTROSTATIC MEMS

This chapter discusses the mathematical modeling component, a process in which real-world situations and their relationships are expressed mathematically or in which real-world problems are translated into mathematical language, solved within a mathematical system, and solutions tested again within the real-world system. This chapter will derive the MEMS mathematical model based on the Parallel Plate beam equation. After that, we will simplify the model to the equivalent spring mass damper equation to make things easier to understand. In addition, we will discuss a few phenomena associated with MEMS, such as pull-in, hysteresis, stiction, and damping.

2.1 MEMS Electrostatic Parallel Plate Model

Electrostatic MEMS as a parallel plate refers to a specific type of technology that uses parallel plate capacitors as a key component. These devices are designed with two flat, conductive plates positioned parallel and separated by a tiny gap. Imagine two flat plates, like tiny sheets of metal, placed close together but not touching. The top plate can move or be controlled while the bottom plate remains still. The gap between the plates is very small, on micrometers or nanometers. The movable plate can be pushed or pulled by an external

force or using special mechanisms like electricity or vibrations. When the movable plate moves, it changes the space between the plates, affecting capacitance. Capacitance is a measure of how much electrical charge a capacitor can hold. In this case, the parallel plates act as a capacitor, and the distance between them determines the capacitance. When the movable plate moves, it changes the distance between the plates, which, in turn, changes the capacitance. These changes in capacitance can be detected and used for different purposes. Figure 2.1 illustrates the MEMS schematic as the parallel plate.

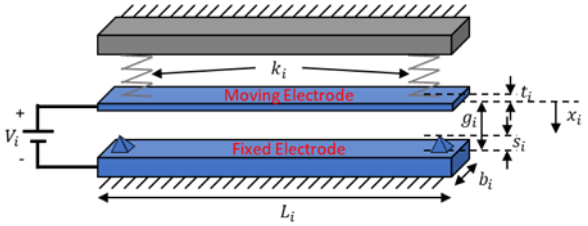

Figure 2.1: MEMS schematic diagram.

For modeling the MEMS as a parallel plate, the electrostatic force resulting from the applied voltage signal across the electrodes is defined as:

$$F_{P.P.} = \frac{\varepsilon A[V_{DC}+V_{A.C.}\cos(\Omega t)]^2}{2(g-x)^2} \quad (2.1)$$

where:

x: The beam deflection.

ε: Represents the permittivity of the material between the conductive components.

A: The electrode area

Ω: represents the A.C. signal frequency.

t: represents the time.

V_{DC}: The DC bias voltage applied.

V_{AC}: The A.C. signal applied.

g: represents the initial gap between the electrodes.

The interaction of electric charges causes the electrostatic force in MEMS. An electric field is created between two conducting components separated by a short distance when an electric potential difference (voltage) is applied. This electric field creates opposing charges on the conductive components' surfaces, resulting in an electrostatic force of attraction between them.

2.2 Beam Equation

The moving plate of the MEMS parallel plate can be approximated as a beam. A Beam or Bernoulli-Euler equation is the mathematical representation of how a beam responds in the presence of a load and can be used to describe the MEMS motion. The equation is based on a few assumptions. These include the beam shape or geometry not changing significantly while applying a load. Also, the beam's cross-section is assumed to remain planner and normal to the deformed axis of the beam. Our work will be based on the Cantilever beam model. Cantilever is a type of beam that has been fixed from one side and free from the other side, as shown in Figure 2.2

Assuming the applied force is a uniform distributed load over the beam, the deflection is defined as:

$$\delta = \frac{wL^4}{8EI} \tag{2.2}$$

Where:

δ: The deflection at the tip in m

w: Load in kN/m

L: Beam length in m

E: Young's Modulus in MPa

I: The beam moment of inertia in m^4

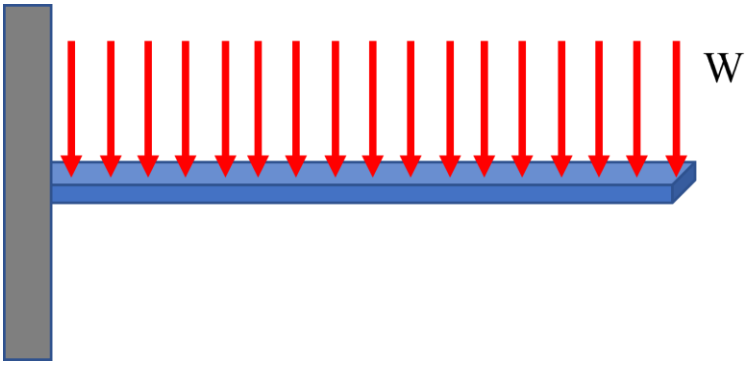

Figure 2.2: Cantilever beam schematic.

If the deflection of the beam at the tip, which would have the largest deflection, is of interest, a set of ordinary differential equations can be used as follows based on Equation 2.2. On the other hand, beam equation can be written as a partial differential Equation if interest is on the beam deflection over the position along the beam and time, as shown in equation 2.3:

$$E.I.\frac{\partial^4 w}{\partial x^4} + \rho A\frac{\partial^2 w}{\partial t^2} + c\frac{\partial w}{\partial t} - N\frac{\partial^2 w}{\partial x^2} = F \tag{2.3}$$

where:

E: Young's Modulus in MPa

I: The beam moment of inertia in m^4.

ρ: Beam material density in kg/m^3.

A: Beam cross-sectional area in m^2.

c: damping coefficient in Ns/m.

F: Applied force in Newton.

Besides the mathematical representation of the beam equation, a more simplified representation can be used. This representation is based on the spring mass damper system formula. This representation provides a useful approximation that simplifies the analysis and helps us understand the dynamic behavior of beams, as we will discuss in the following section.

2.3 Spring Mass Damper Model

Instead of using the beam's high-order partial differential equation to describe the beam's dynamics and behavior under different loads or constraints, a simplified spring mass damper system representation, as shown in Figure 2.3, can be used. The spring-mass damper system is based on a set of ordinary differential equations, which is less challenging on the computing side and even easier to understand and track. Also, the spring mass damper system is a very useful representation to study the dynamic behavior of the beam,

finding and analyzing some important parameters such as the damping coefficient and the response at the resonance frequency. Moreover, we can study these parameters in the presence of different types of loads, which helps us understand different cases and gives us more flexibility to predict the system's behavior with different parameters.

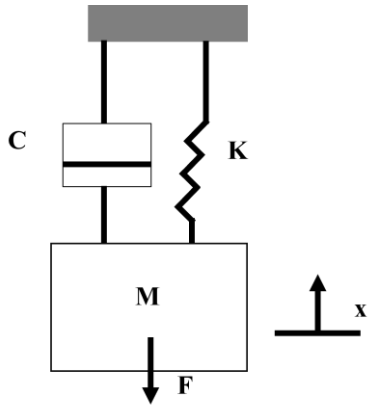

Figure 2.3: Spring-mass damper schematic.

For the spring mass damper system, the equation of motion can be find using Newton second law as:

$$\sum F=ma \tag{2.4}$$

$$m\ddot{x} + c\dot{x} + kx = F \tag{2.5}$$

where:

m: is the proof of mass in kg.

c: is the damping coefficient in Ns/m.

k: is the spring stiffness in N/m.

F: is the applied force in N.

2.4 Single Degree of Freedom Model Parameters

Here we present a detailed explanation of extracting the single-degree model parameters, such as the equivalent mass and stiffness for the beam and the electrostatic force.

The equation of motion states that the sum of the forces acting on the plate is equal to the mass times the acceleration of the plate. In this model, we assume that the movable plate can be represented as a single-degree-of-freedom system, with its motion along one direction, denoted by x. The equivalent mass of the movable plate is denoted by m, and the equivalent stiffness of the beam supporting the plate is denoted by k. The damping coefficient, c, accounts for any dissipation of energy in the system. The equation of motion for the MEMS device is

$$m\ddot{x} + c\dot{x} + kx = F \tag{2.6}$$

Combining the effective mass and the equivalent stiffness for the beam to this model, assuming that m_{eff}=0.646m and $k_{eq}=\frac{8EI}{L^3}$.[30]

So, our final model is shown as:

$$0.646\ m\ \ddot{x} + c\dot{x} + \frac{8EI}{L^3}x = \frac{\varepsilon A[V_{DC}+V_{A.C.}\cos(\Omega t)]^2}{2(d-x)^2} \tag{2.7}$$

Where:

E: Young's Modulus in MPa

I: The beam moment of inertia in kg/m^2.

L: Beam length in mm.

ε: Represents the permittivity of the material between the conductive components.

A: The electrode area

V_{DC}: The DC bias voltage applied.

V_{AC}: The A.C. signal applied.

d: represents the initial gap between the electrodes.

2.5 Pull-in Bi-stability Phenomenon

A DC voltage is applied to the beam in microelectromechanical systems, causing it to deflect. An A.C. signal can also be used if the deflection is required to have an oscillating motion about that point. This can aid in analyzing MEMS behavior by providing more parameters to investigate. Both DC and A.C. loads have an upper limit beyond which the mechanical restoring force of the beam can no longer resist the opposing force, resulting in a continuous increase in beam deflection, which increases the electrostatic force until contact occurs between the beam and fixed electrode. This instability behavior is called Pull-in, and the voltage associated with reaching this behavior is called Pull-in voltage. If a D.C. signal was applied to the beam, it resulted in a static pull-in, whereas an A.C. signal resulted in a dynamic pull-in behavior. A stopper is added to eliminate a short circuit between the beam and the fixed electrode. Figure 2.4 shows a beam under the pull-in.

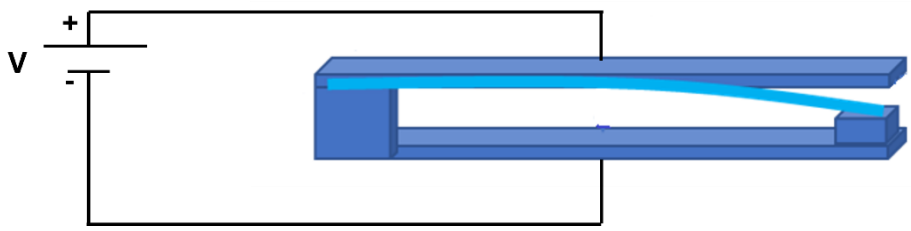

Figure 2.4: Beam under pull-in.

2.6 Hysteresis Phenomena

In the context of MEMS, hysteresis plays a crucial role in their working principles. Hysteresis in MEMS refers to a phenomenon where the system's response, such as a material or structure, is dependent on the current input force or deformation and its history. Specifically, when a force or voltage is applied to a material, causing it to undergo deformation in the forward direction, hysteresis manifests as a nonlinear behavior during the subsequent reduction of the force. More specifically, when the applied force is decreased, the material's deformation does not follow the exact reverse path of the initial forward deformation. Instead, the material exhibits a lag or memory effect, resulting in a different deformation path during the force reduction compared to the forward path. This behavior is characteristic of hysteresis in MEMS. Integrating this explanation with the previous definition, we can provide a revised and more comprehensive description: Hysteresis, in general, refers to the phenomenon where the response of a system depends not only on its current input but also on its history or past inputs. In the context of MEMS, hysteresis becomes a significant factor in the system's working principles. When a certain type of force is applied to a material or structure within a MEMS device, causing it to undergo deformation in the forward direction, hysteresis manifests as a nonlinear behavior during the subsequent force reduction. The material's deformation during force reduction does not follow the exact reverse path of the initial forward deformation but exhibits a lag

or memory effect. This behavior is known as hysteresis in MEMS, and it influences the performance and characteristics of the MEMS network. Figure 2.2 shows the hysteresis loop behavior in MEMS.

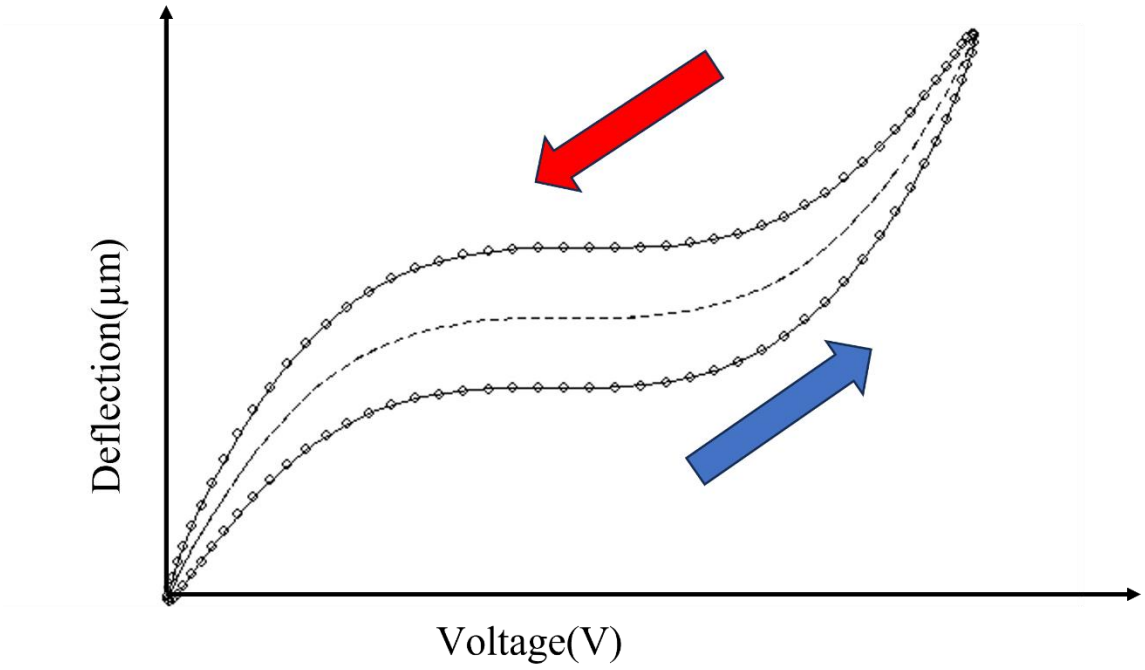

Figure 2.5: Hysteresis loop curve.

2.7 Damping Effect

We include the damping effect in the simplified model for the MEMS device with a single degree of freedom because we want to account for energy dissipation within the system. The device's dynamic behavior and stability are directly influenced by damping, which plays an essential role in both aspects. The damping coefficient, denoted by the letter c in

the equation of motion, is responsible for the resistance to motion that damping provides. It is responsible for lowering the magnitude of oscillations and managing the rate at which the moveable plate returns to its original position after the disruption. The effectiveness of the damping effect is directly proportional to the magnitude of the damping coefficient, denoted by the letter c. A higher damping coefficient results in a more severe energy loss and faster decay of oscillations. The reduction in the frequency of oscillations causes both of these effects. On the other hand, if the damping coefficient is smaller, the system can continue oscillating for longer before coming to rest.

In the result chapter, we will talk more about how the damping ratio would affect the damping coefficient, which could result in a system that works as intended or one that fails to do the task asked of it.

2.8 Stiction Effect

Capillary forces are one of the sources of nonlinearities in MEMS. This force can be due to humidity, leading to stiction. In this section, the stiction effect was studied and molded. Wet conditions can come from wet etching, an important process to remove the sacrificial layers to ensure the release of the microstructures from the substrate [30].

In the beginning, we assumed that the only force affecting the system is the electrostatic force, so, at pull-in, the restoring force that pulls the system away from the pull-in is the beam's stiffness and the stopper's reaction force F_r. Both dynamic and steady-state schematic of the beam are shown in Figure 2.6.

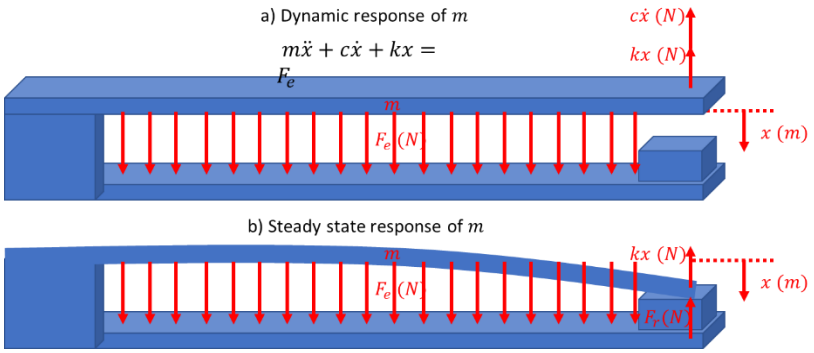

Figure 2.6: a) Dynamic response free body diagram. b) Static response free body diagram at pull-in.

Equation 2.8 represents the beam's dynamic response, while equations 2.9 and 2.10 are for the static equilibrium at the pull-in state:

$$m\ddot{x} + c\dot{x} + kx = F_e\,, \qquad \text{At steady state: } \ddot{x} = \dot{x} = 0 \tag{2.8}$$

$$kx_{@pull-in} = F_{e@pull-in} + F_r\,, \quad \text{where } F_r \text{ can never be } F_r \geq 0 \tag{2.9}$$

$$F_e = \frac{\varepsilon A V^2}{(g_0 - x)^2} \quad \text{and} \quad F_{e@pull-in} = \frac{\varepsilon A[V_{DC} + V_{A.C.}\cos(\Omega t)]^2}{(g_0 - x_{@pull-in})^2} \tag{2.10}$$

where x is the beam's tip deflection and $x_{@pull-in}$ is the stopper height. m, c, and k are the mass, damping constant, and stiffness of the beam, respectively. F_r is the normal reaction force of the stopper. F_e is the electrostatic force, $\varepsilon = 8.854 \times 10^{-12}$, A, V, and g_0 are the absolute permittivity of air, the overlapping area between the two electrodes, the input voltage, and the initial gap between the electrodes at rest position, respectively.

To maintain the pull-in, all forces acting toward the pull-in must be greater than or equal to the stiffness restoring force ($kx_{@pull-in}$). Since the only force assumed to act toward the pull-in is the electrostatic force, then $F_e \geq kx_{@pull-in}$ is required to maintain the pull-in. To release the system (pull-out), the electrostatic force F_e should be decreased to

achieve $F_e < kx_{@pull-in}$, which can be done by decreasing the input voltage ($F_e = \frac{\varepsilon A[V_{DC}+V_{A.C.}\cos(\Omega t)]^2}{(g_0-x_{@pull-in})^2}$).

Theoretically, if the electrostatic force is set to zero ($F_e = 0$), the beam must release and never get stuck). However, based on initial testing in ambient air, some designs stick at the pull-in and never release even at zero input voltage ($F_e = 0$). This brings us to question the claim that F_e is the only force acting on the system toward the pull-in? Specifically, due to wet etching by some acidic liquids during fabrication and the fact that the beams are operated in the room environment, there is a good chance of wet adhesion sticking forces (capillary force). Stepping further into this hypothesis, we introduce a capillary sticking force to our model, see Figure 2.7 and Equation 2.11:

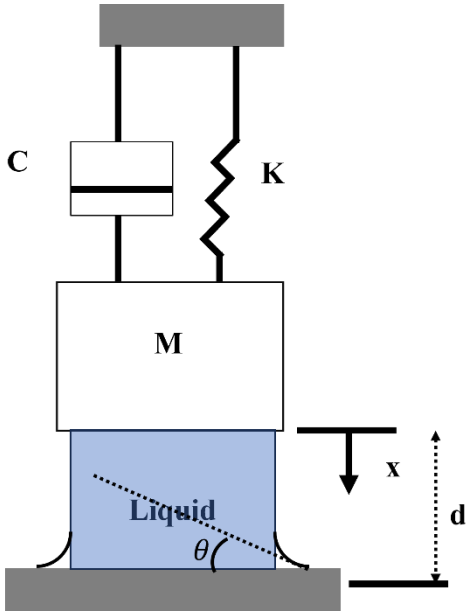

Figure 2.7: Spring mass system under capillary stiction force (wet adhesion).

$$F_{cap} = \frac{2\gamma A_{cap}\cos(\theta)}{(d-x)} \quad (2.11)$$

where:

γ: is the surface tension for the liquid ($\gamma = 0.073 N/m$ for water)

θ: is the angle that the liquid makes between the beam and the substrate (assume perfect wetting with $\theta = 0°$)

d: is the thickness of the liquid layer.

A_{cap} : is the area of the beam that is in contact with the water (we will assume $A_{cap} = aA$ and vary the ratio $a \sim (0 - 0.2)$.

Figure 2.8 shows the free-body diagram considering the electrostatic and capillary forces. Since *F*cap is not applied unless pull-in occurs and x can never exceed $x_{@pull-in}$ (beam never penetrates through the stopper, then $x_{@pull-in}$. This leads to 2.12 and 2.13:

$$F_{cap_{@pull-in}} = \frac{2\gamma(aA)}{(g_0 - x_{@pull-in})} \quad (2.12)$$

$$kx_{@pull-in} = F_{e@pull-in} + F_{cap_{@pull-in}} + F_r \quad (2.13)$$

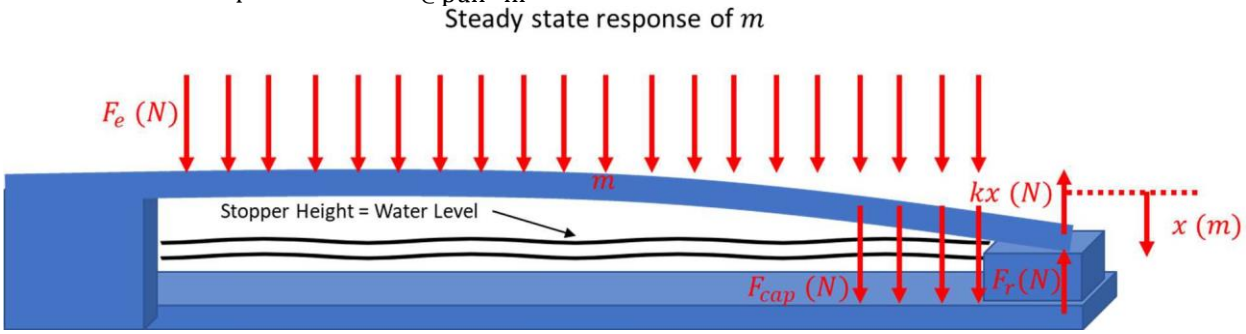

Figure 2.8: Static response free body diagram at pull-in under electrostatic and capillary forces.

Assuming the worst-case scenario of angle ($\theta = 90°$), we need to estimate the water contact area. A good beam design to work for this estimation is the CL900 design, as this design parameters will be discussed in Chapter 4. This beam has been experienced to be stuck for some chips and work fine for others. Using this beam parameter, we manually adjusted the area ratio a until we reached the critical range where a slight change stuck the system. The simulation results will be discussed in the results chapter.

CHAPTER 3

METHODOLOGY

In this chapter, we will discuss our MEMS network's working principles and the signal classification methodology.

3.1 Working Principles and Classification Methodology

This section shows the methodology used to solve the classification problem shown in Figure 3.1. Next, we will explain the signal classification methodology that we used.

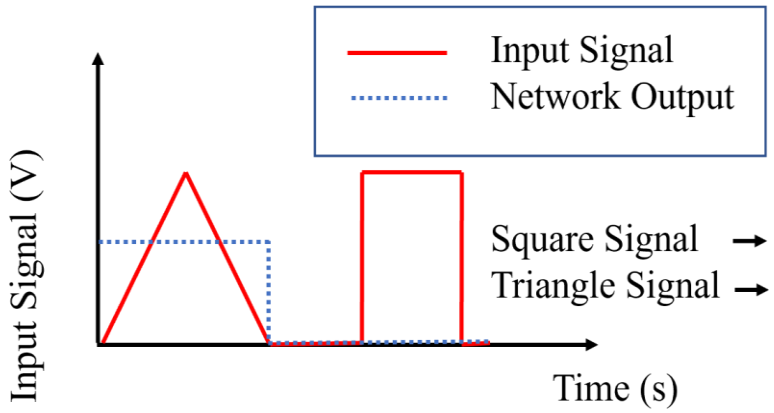

Figure 3.1: Square vs triangle waveform classification problem.

When a triangle signal is applied as the actuation voltage, the first input MEMS device pulls in, and its positive coupling with the output MEMS O_3 also results in pulling it in, as shown in the sequence starting from Figure 3.2 to Figure 3.5.

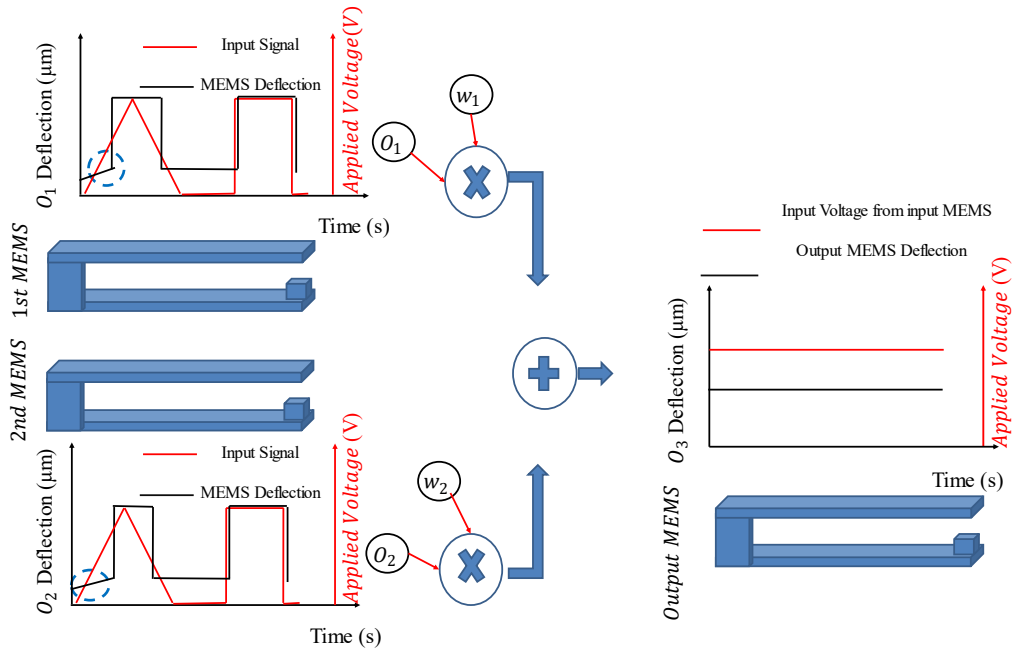

Figure 3.2: MEMS network diagram before at the beginning of signal.

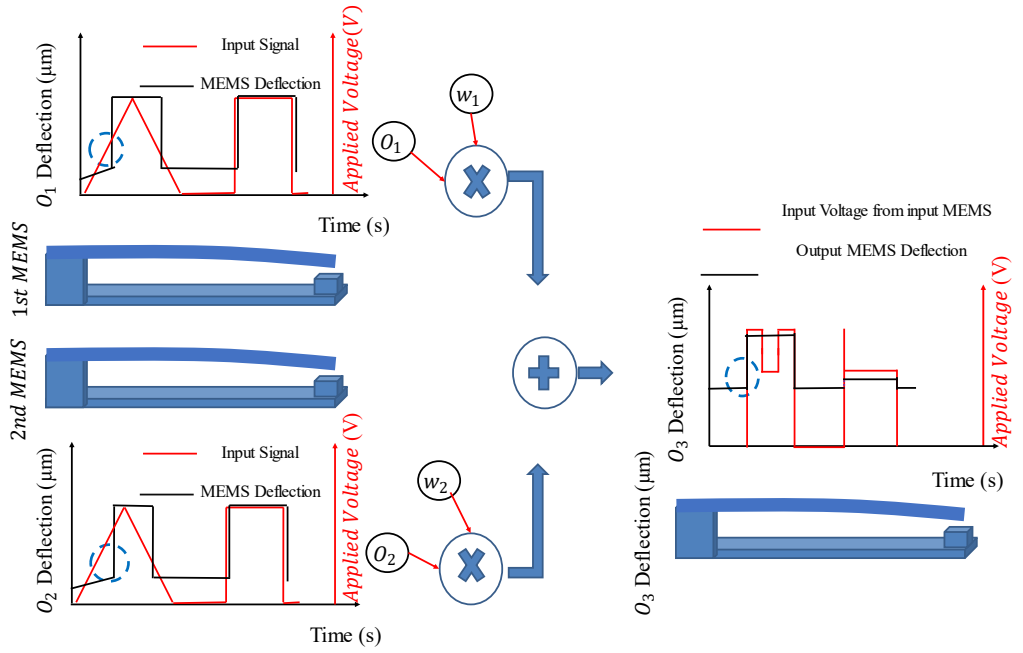

Figure 3.3: Both input MEMS start to deflect while increasing the input voltage.

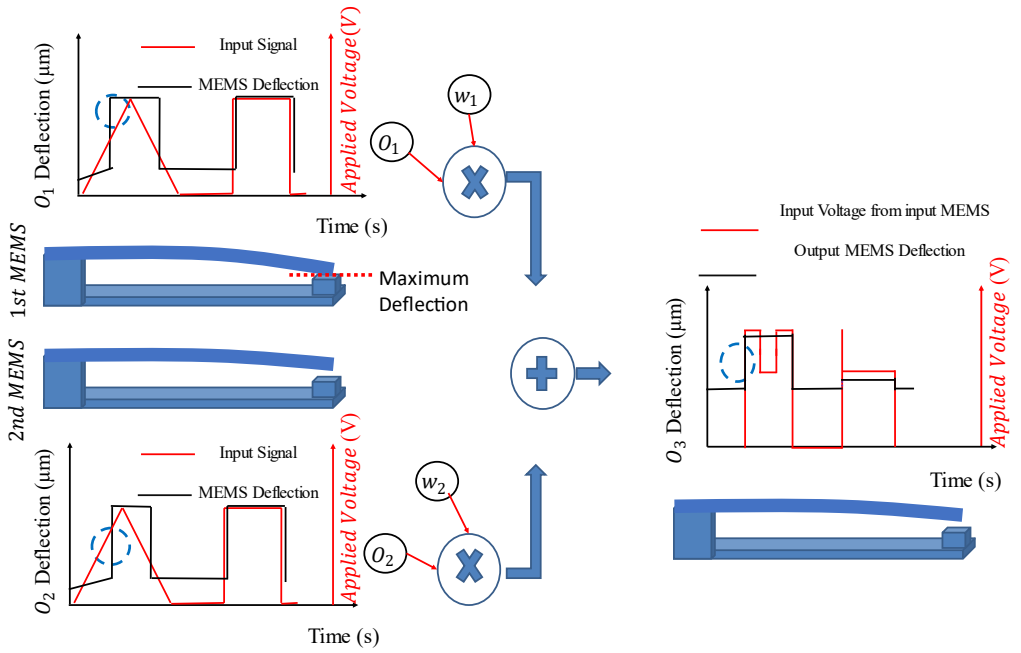

Figure 3.4: First MEMS reached the pull-in.

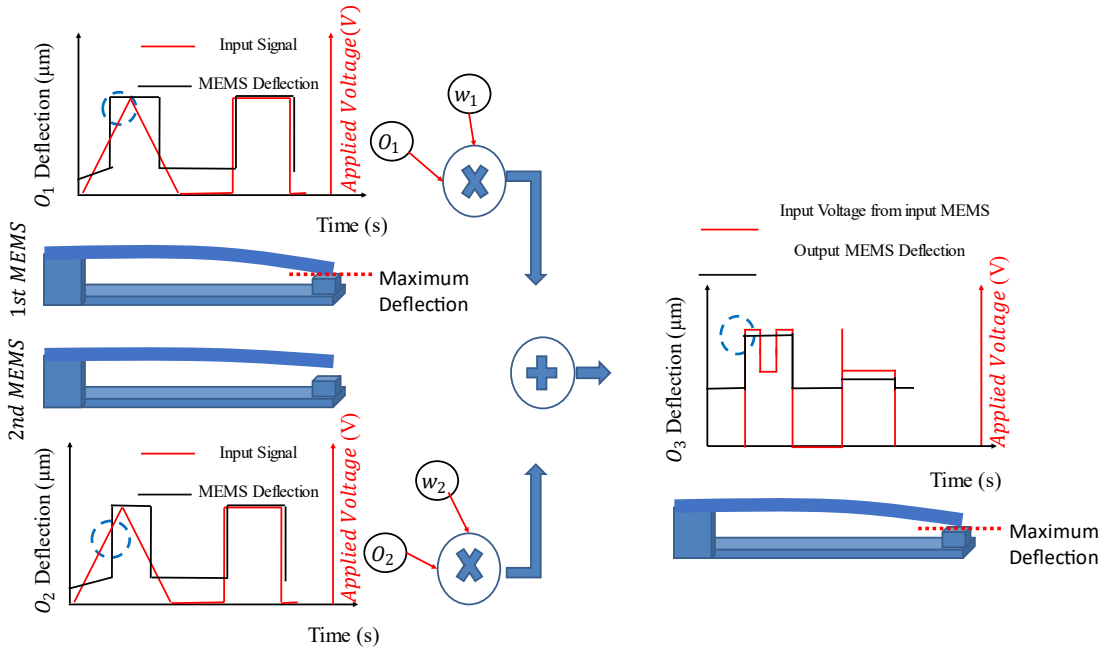

Figure 3.5: Output MEMS reach the pull-in due to the voltage coming from the first MEMS.

As the voltage continues to increase, I_2 will also reach the pull-in, resulting in an output multiplied with a negative weight as in input to the output MEMS O_3. However, due to bi-stability hysteresis, O_3 remains pulled in due to the effective voltage acting upon it, as shown in Figure 3.6 and 3.7.

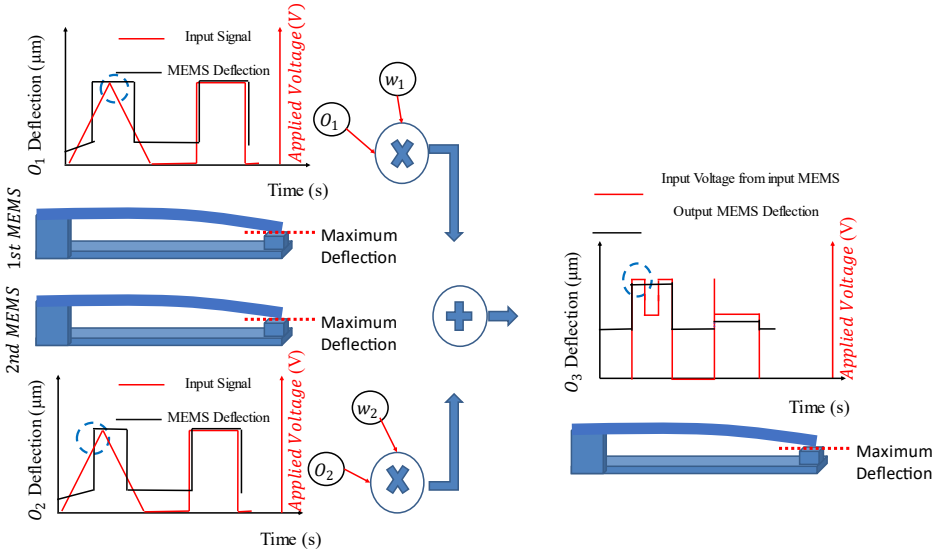

Figure 3.6: 2nd MEMS at pull-in.

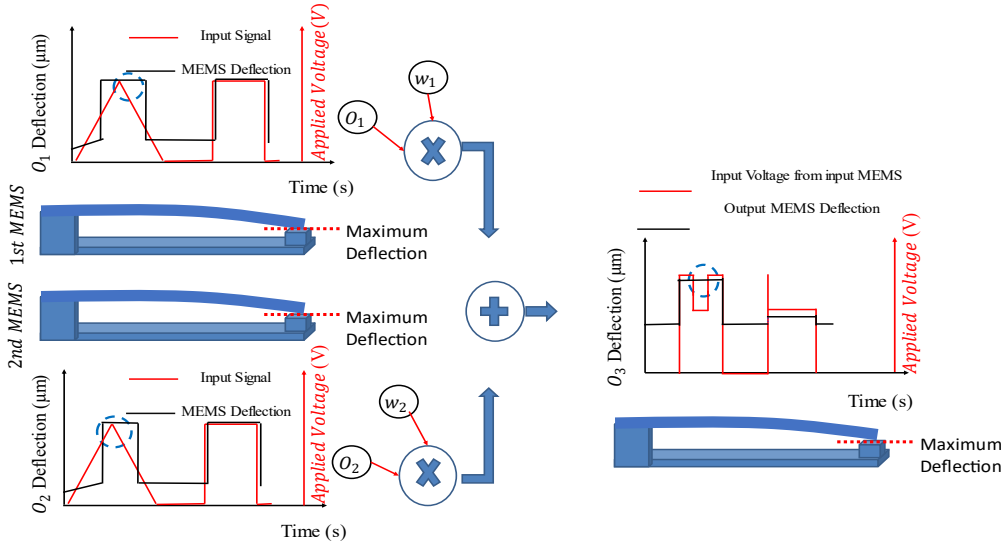

Figure 3.7: Output MEMS at pull-in due while the input voltage decreased due to 2nd MEMS pull-in.

And then the applied voltage signals will keep decrease, the 2nd MEMS will release first, then the 1st MEMS release too which makes the output MEMS release as shown in Figure 3.8,3.9 and 3.10.

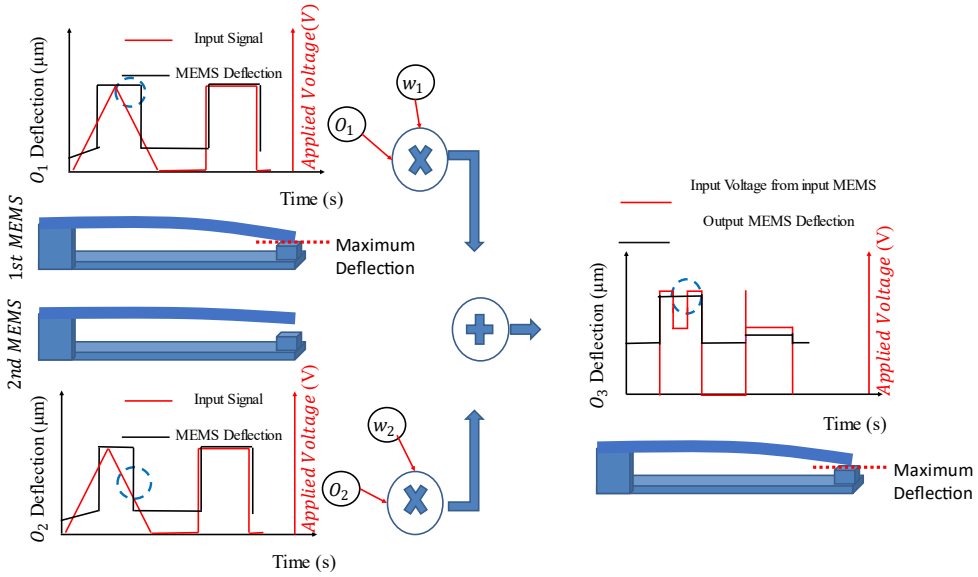

Figure 3.8: 2nd MEMS at pull-out (release) due to the failing edge of the input signal.

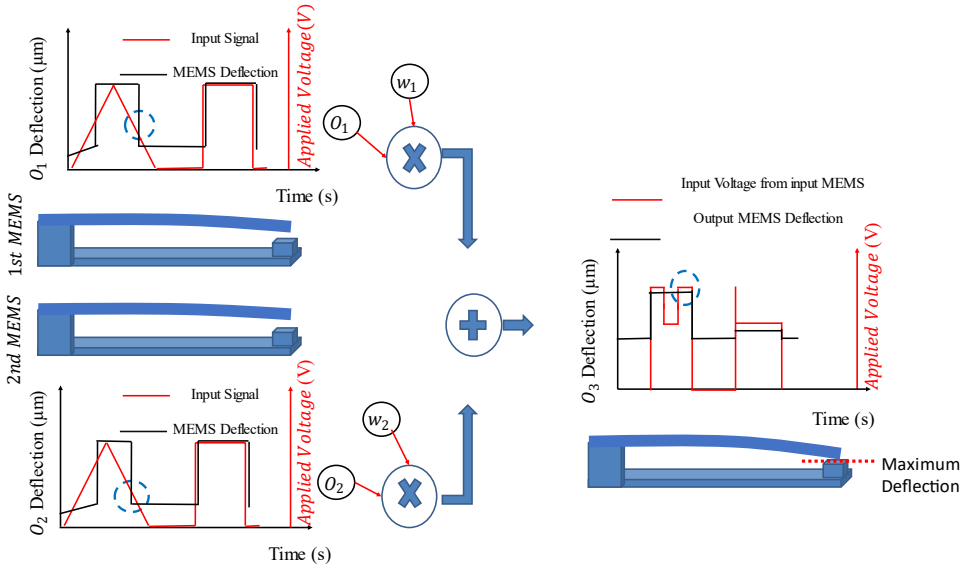

Figure 3.9: 1st MEMS at pull-out (release) due to the failing edge of the input signal.

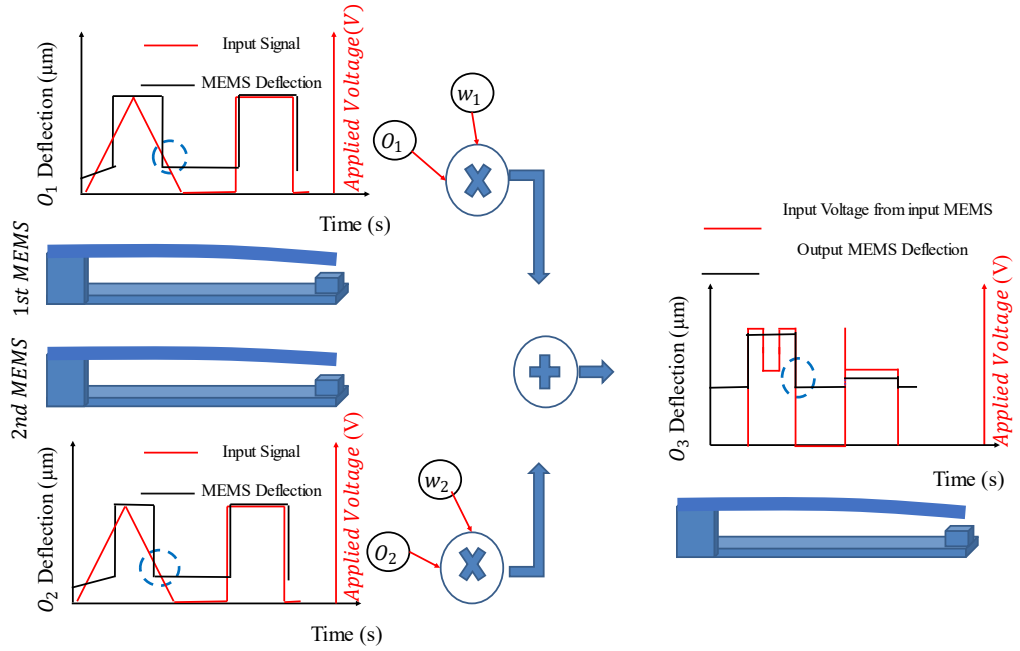

Figure 3.10: Output MEMS at pull-out (release) because no voltage is applied fro the input MEMS .

On the other hand, when a square signal is applied, both I_1 and I_2 pull in simultaneously. The combined effective voltage exerted by these input devices on O_3 cannot cause a pull-in response. Figure 3.11 to Figure 3.14 show the MEMS network and a schematic for the classification task based on the square signal.

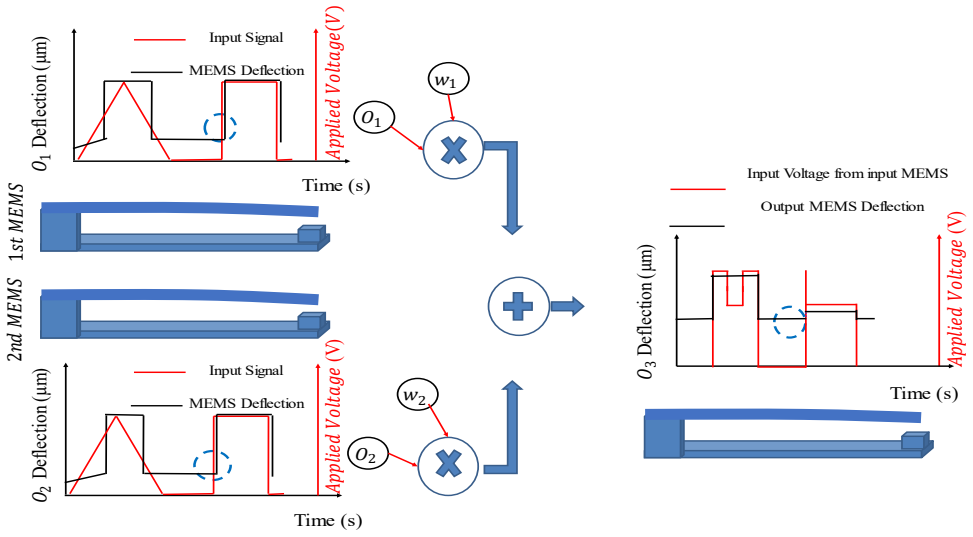

Figure 3.11: Applying square signal for the input MEMS .

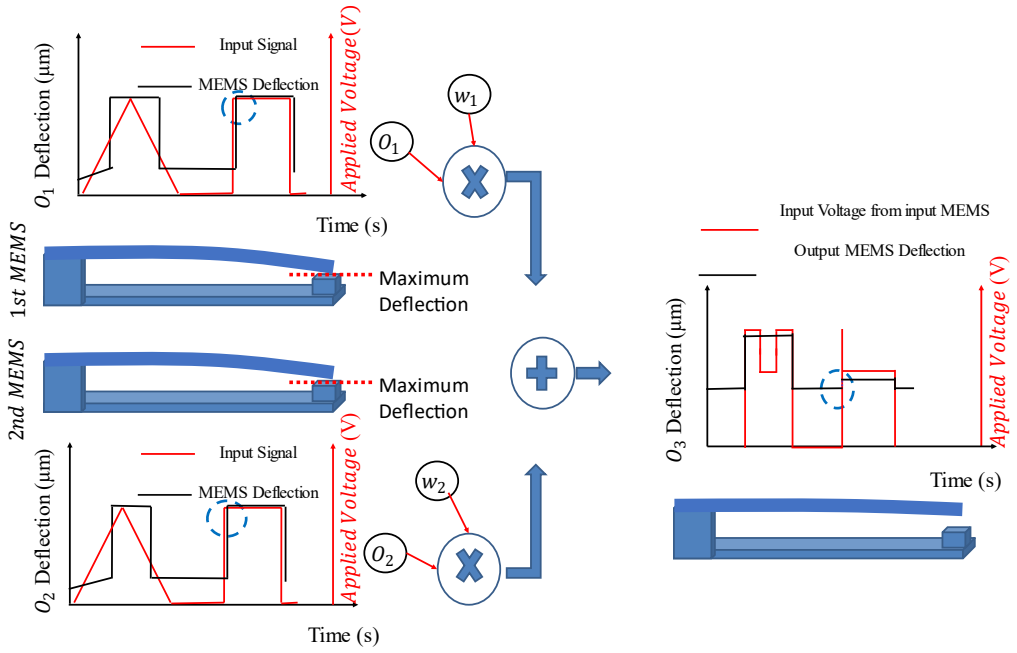

Figure 3.12: Both input MEMS reach the pull-in due the the rapid shape of square signal .

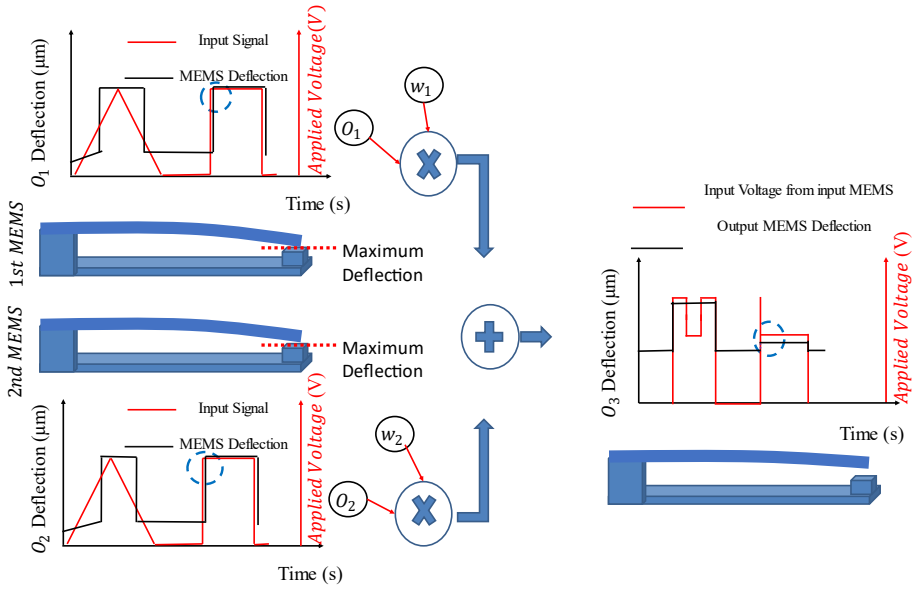

Figure 3.13: Both input MEMS at pull-in will generate a voltage that is not enough to make the output MEMS reach the pull-in .

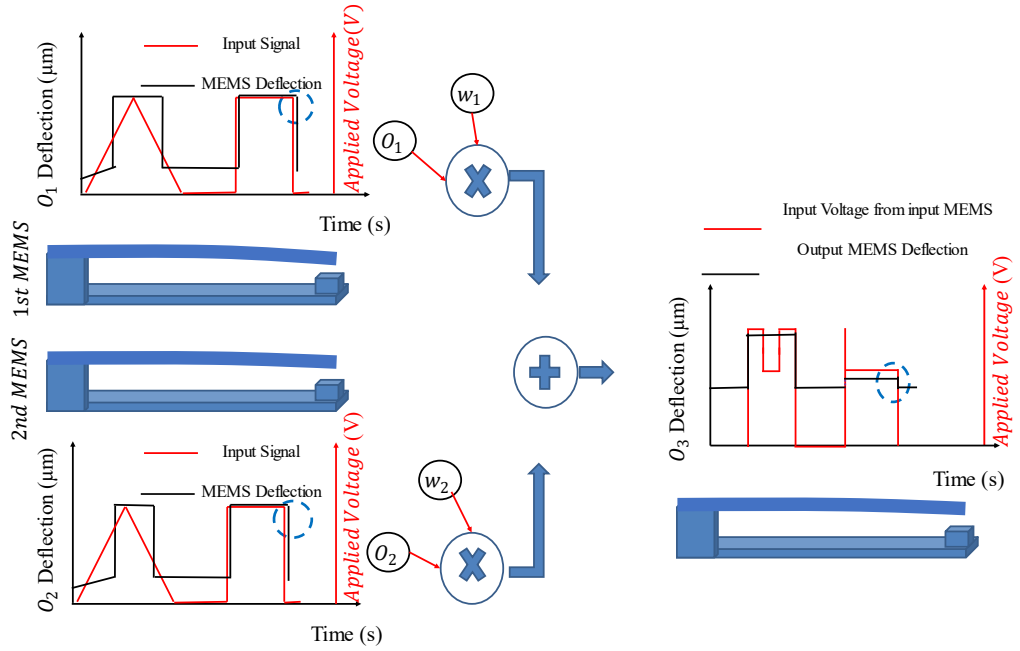

Figure 3.14: Output MEMS didn’t pull-in while the input MEMS reach pull-in .

By observing the pull-in behavior and the resulting status of the output MEMS device, the network effectively classifies the input signals. The distinct responses exhibited by the MEMS devices within the network provide a reliable basis for signal classification. To differentiate between triangle and square signals, this method makes use of the unique characteristics and hysteresis features of MEMS devices. This interconnected methodology ensures the network's response to different input signals is well understood and provides a robust foundation for accurate signal classification.

CHAPTER 4

MEMS DESIGN

This chapter summarizes the MEMS design steps, where a cantilever design was proposed with different parameters to find the optimal design that satisfies our needs.

4.1 Cantilever Design

In this section, we aimed to find the optimal parameters for our Cantilever to make our MEMS network capable of the classification task. We tried to have more than one design due to fabrication limitations. The design and optimization steps were done using MATLAB. A wide range of values for each beam parameter was performed to ensure we have as many working designs as possible.

Figure 4.1 shows the cantilever schematic and the parameters we used for the design. Also Table 4.1 summarizes the different working designs and their parameters.

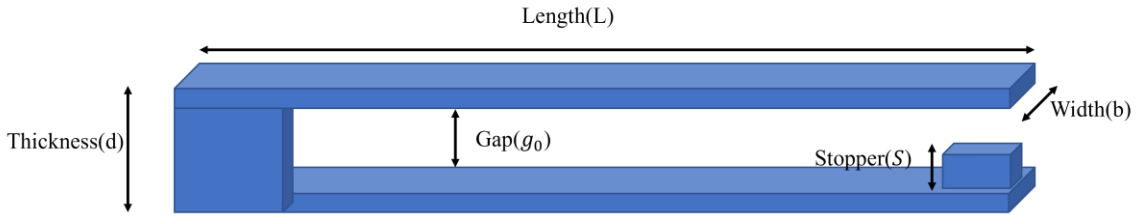

Figure 4.1: Cantilever beam with parameters.

Table 4.1: Summary of Cantilever different design parameters.

Design	L	b	g_0	d	S	V_{bi1}	V_{bi2}	V_{bout}	W_1	W_2	V_{in}
	[um]	**[um]**	**[um]**	**[um]**	**[um]**	**[V]**	**[V]**	**[V]**			**[V]**
CL400	400	100	3	6	1.25	14	9	17	1	-.75	20
CL500	500	100	4	6	1	14	9	17	1	-.75	20
CL600	600	100	5	6	2	14	8	17	1	-.75	20
CL700	700	100	5	6	1.5	10	6	13	1	-.75	15
CL900	900	100	5	6	1.5	7	4	7	1	-.75	10
CL1000	1000	100	5	6.1	1.25	5	3	6	1	-.75	10
CL1500	1500	100	5	7	2	4	2	2	1	-.75	5
CL2000	2000	100	15.2	7	3.8	9	7	11	1	-.75	10

4.2 CL900 Design

We found that the stiction force plays a major role in determining the suitable working design. Whereas we increase the contact area a_c between the beam and moisture, the chance to reach the pull-in and stick increases as shown in Figure 4.2.

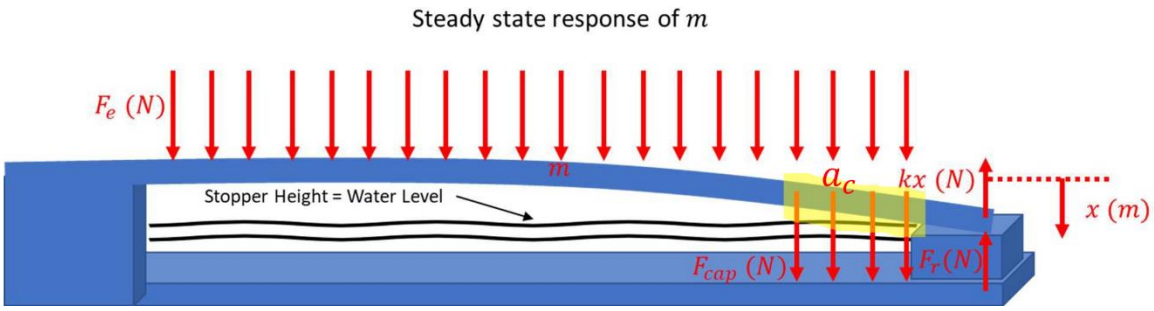

Figure 4.2: Cantilever beam with the presence of capillary force(stiction).

As a result, we found that the CL900 design can be considered the best working design in the presence of stiction force. All designs with higher lengths tend to be stuck without release, as shown in Table 4.2.

Table 4.2: Summary of Cantilever different design parameters with restoring force.

Design	L	b	g_0	d	S	K	MaxRestoringForce	a_c
	[um]	**[um]**	**[um]**	**[um]**	**[um]**	**[N/m]**	**[uN]**	**[10^{-6}]**
CL400	400	100	3	6	1.25	34.65	60.63	5519
CL500	500	100	4	6	1	17.74	53.22	468
CL600	600	100	5	6	2	10.26	30.80	3620
CL700	700	100	5	6	1.5	4.65	22.62	875
CL900	900	100	5	6	1.5	3.04	10.64	227
CL1000	1000	100	5	6.1	1.25	2.33	8.73	50
CL1500	1500	100	5	7	2	1.04	3.13	43

CL2000	2000	100	15.2	7	3.8	0.44	5.01	6

From table 4.2, we found that when the contact area ratio a_c exceeds a value of $227*10^{-6}$, the beams never release due to the capillary force. Also, CL900 design gives us the highest capacitance change reflected in the deflection compared to the other working designs.

CHAPTER 5

Discussion and Results

In this chapter, we present the discussion and results of our research on signal classification based on analog computing using a MEMS network. We successfully developed and implemented the MEMS network for signal classification tasks and conducted several case studies to investigate the impact of various parameters on classification performance. The findings provide valuable insights into the capabilities and behavior of the MEMS network and shed light on its potential for signal classification applications.

5.1 Successful Signal Classification

Our investigation demonstrated that the MEMS network can achieve successful signal classification. By harnessing the analog computing capabilities of the MEMS devices, we effectively processed and interpreted input signals, achieving accurate classification results. This outcome validates the viability of the MEMS network as a promising solution for signal classification tasks. Figure 5.1 shows the MEMS network response to both triangle and square signals. As shown, we can see that as a triangle signal is applied on the first MEMS, at the pull-in voltage, the MEMS reaches the pull-in as it has the maximum deflection available. Then the output from the first MEMS is multiplied by a positive gain and fed to the output MEMS which also reached the pull-in. When the second MEMS

reaches the pull-in too, the output from that MEMS is multiplied by a negative gain and then fed to the output MEMS, as shown in Figure 5.1. The applied voltage on the output MEMS was decreased, but the output MEMS was still in the pull-in position due to the hysteresis effect until the total applied voltage reached the pull-out voltage, then, the MEMS would pull out and back to the original released state.

On the other hand, when a square signal is applied, both input MEMS reach the pull-in simultaneously, but the output voltage from both of them to the output MEMS is not enough to reach the pull-in.

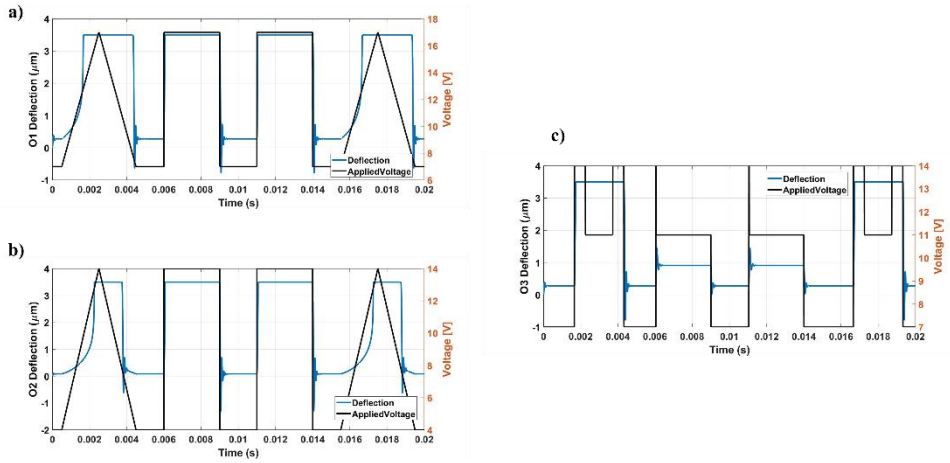

Figure 5.1: a) First MEMS response, b) Second MEMS response, c) Output MEMS response. (The black signals in the figures represents the input voltage applied to each MEMS, while the blue lines represent the deflection)

5.2 Case Studies

To gain deeper insights into the behavior and performance of the MEMS network, we conducted several case studies focusing on parameters that could impact classification outcomes. The case studies encompassed the investigation of capillary sticking force, damping, and varying input signal frequency effects on the pull-in behavior. The findings from each case study are presented below.

5.2.1 Damping Effect Study

The damping effect emerged as a significant factor affecting the classification performance of the MEMS network. We tried different values for the damping ratios ζ, starting with 0.2 until 3.52 as shown in the following figures, Fig.5.2 to Fig.5.4.

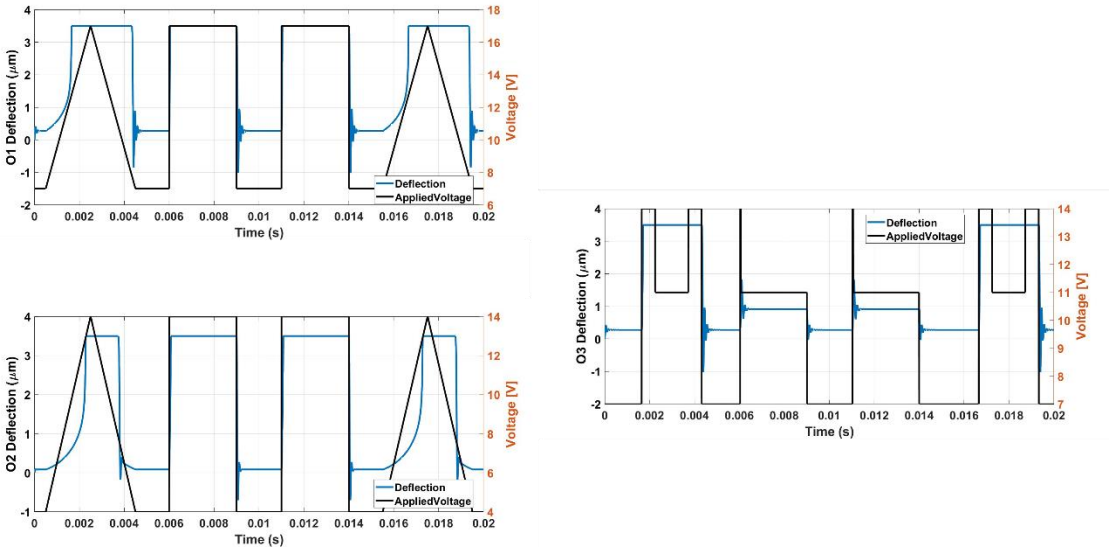

Figure 5.2: MEMS network response with ζ=0.2

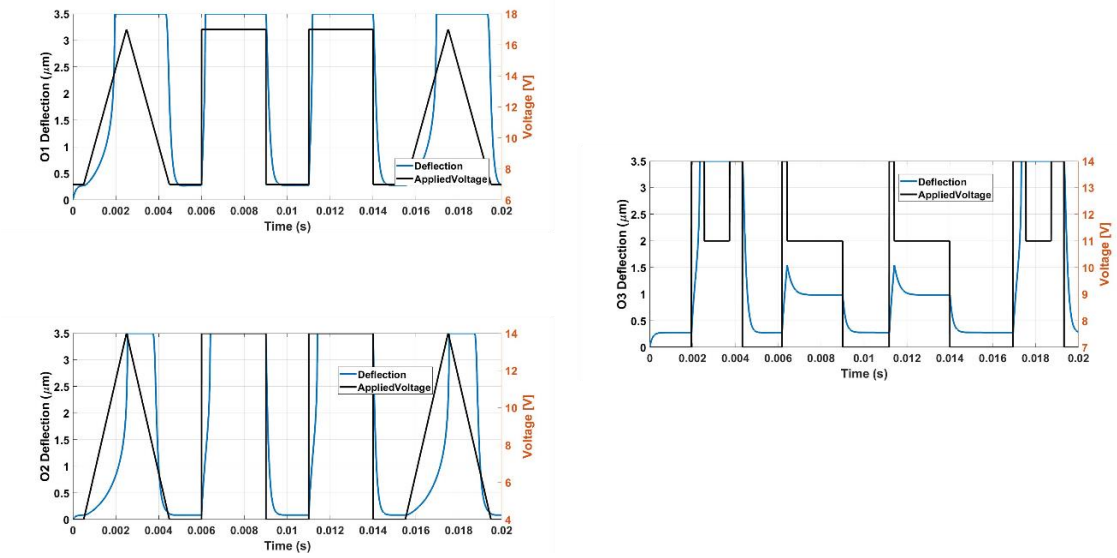

Figure 5.3: MEMS network response with ζ=3.5

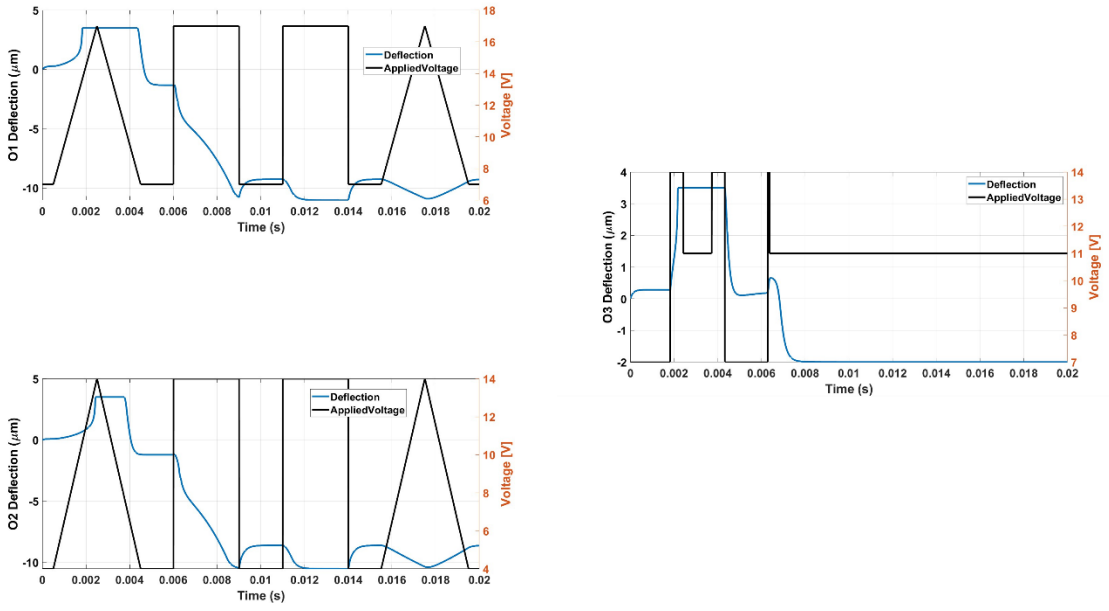

Figure 5.4: MEMS network response with ζ=3.52(The network is not capable of classifying the input signal due to high damping ratio)

From the figures above, we found that within a realistic range of damping ratios, the classification performance of the MEMS network for signal shapes remains largely unaffected until a value for the damping ratio that exceeds 3.52. This analysis showed that the network is robust to damping variations in the context of signal classification.

5.3.2 Varying Input Signal Frequency

Our investigation into varying input signal frequencies uncovered a correlation between signal frequency and classification accuracy. The MEMS network exhibited high accuracy within certain frequency ranges, but deviations were observed at extreme frequency values. Our hypothesis is that for better accuracy, the input signal must have a frequency lower than the MEMS natural frequency. We performed a sweep for the input signal frequency over the cantilever beam designs to validate this hypothesis. Figure 5.5 to Figure 5.20 shows results for a frequency sweep from 200 to 5.6 kHz for the CL900 design.

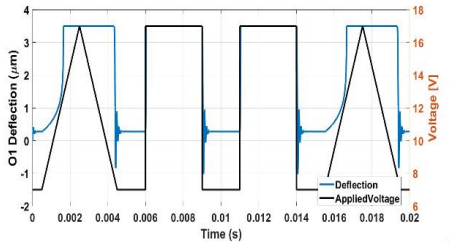

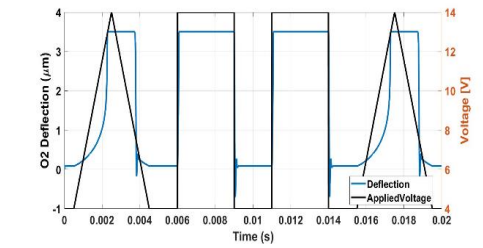

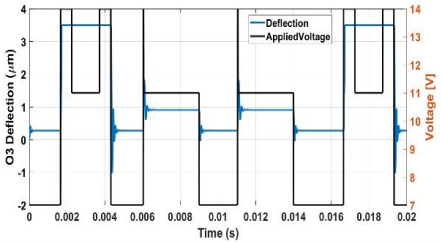

Figure 5.5: MEMS network response with 200 Hz frequency. (O_1 and O_2 pull-in when applying a triangle waveform and pull-out when applying a square waveform, depending on the input MEMS output state. O_3 classifies the input waveform signal.)

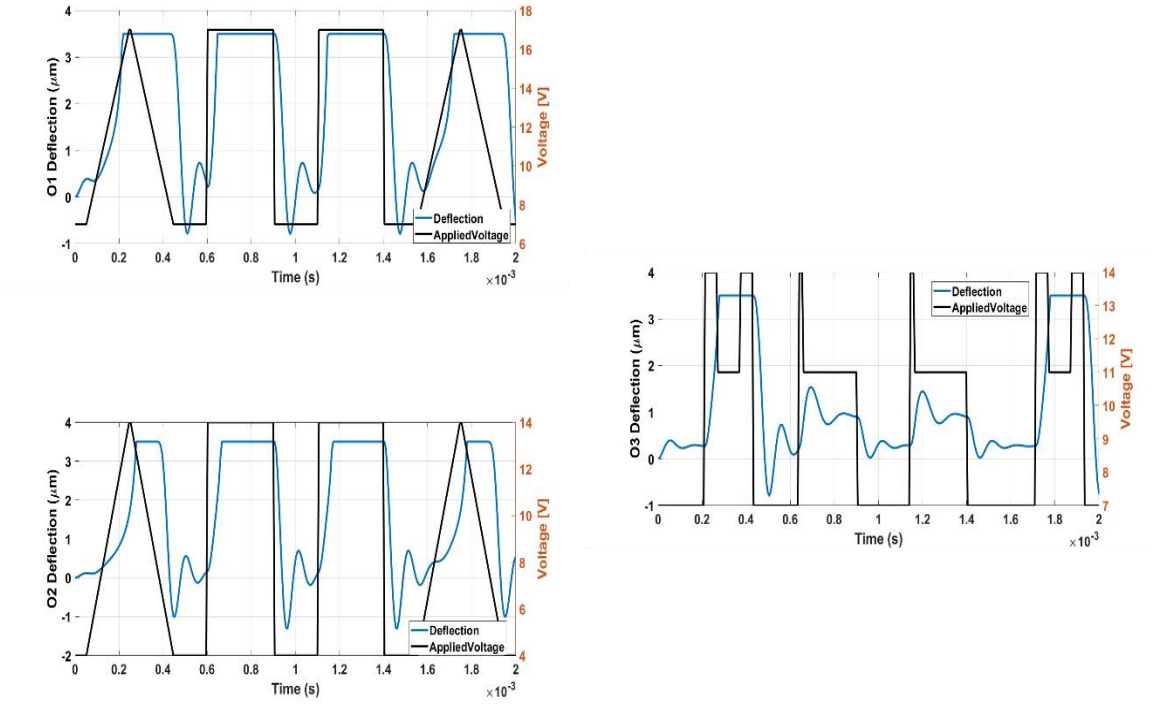

Figure 5.6: MEMS network response with 2000 Hz frequency.(The output MEMS pulls-in for triangle signals and releases for square signals.)

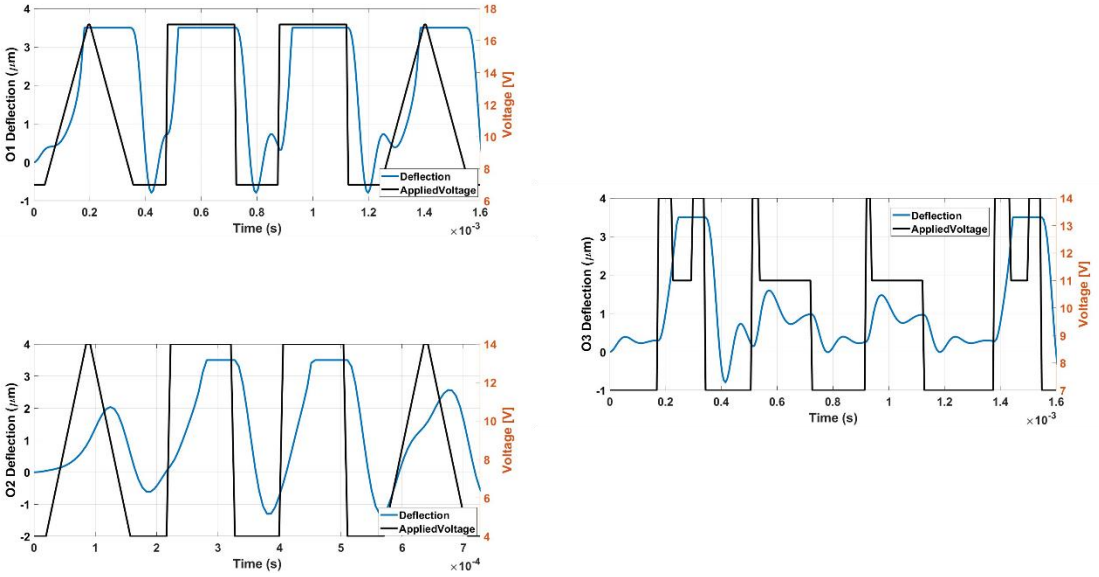

Figure 5.7: MEMS network response with 2500 Hz frequency. (The second input MEMS does not reach pull-in as it should but the output MEMS still pulls-in for triangle signals and releases for square signals.)

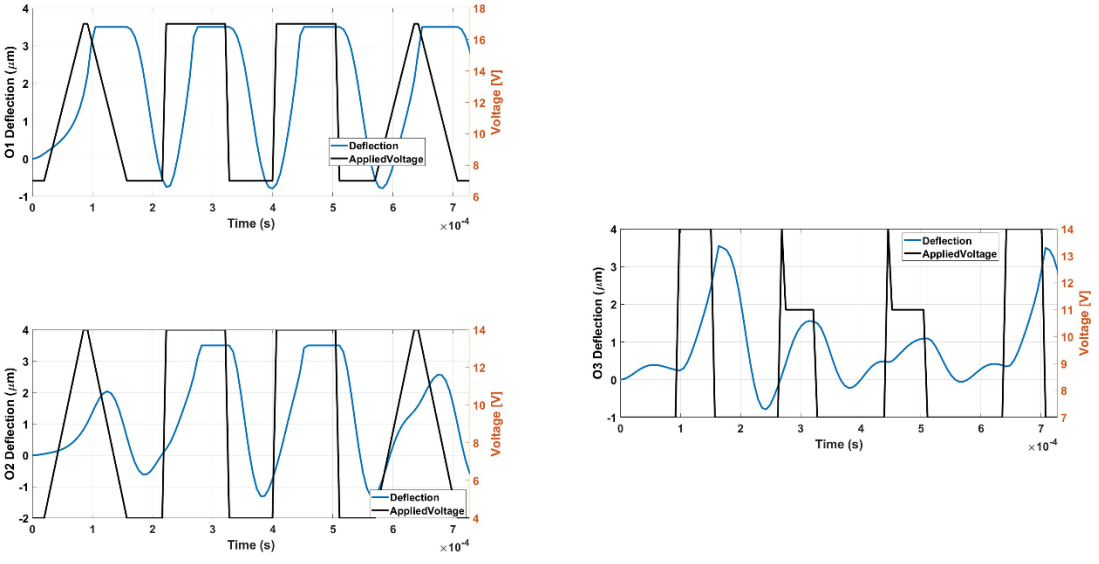

Figure 5.8: MEMS network response with 5500 Hz frequency. (The output MEMS fail to successfully pull-in and classify the input signal.)

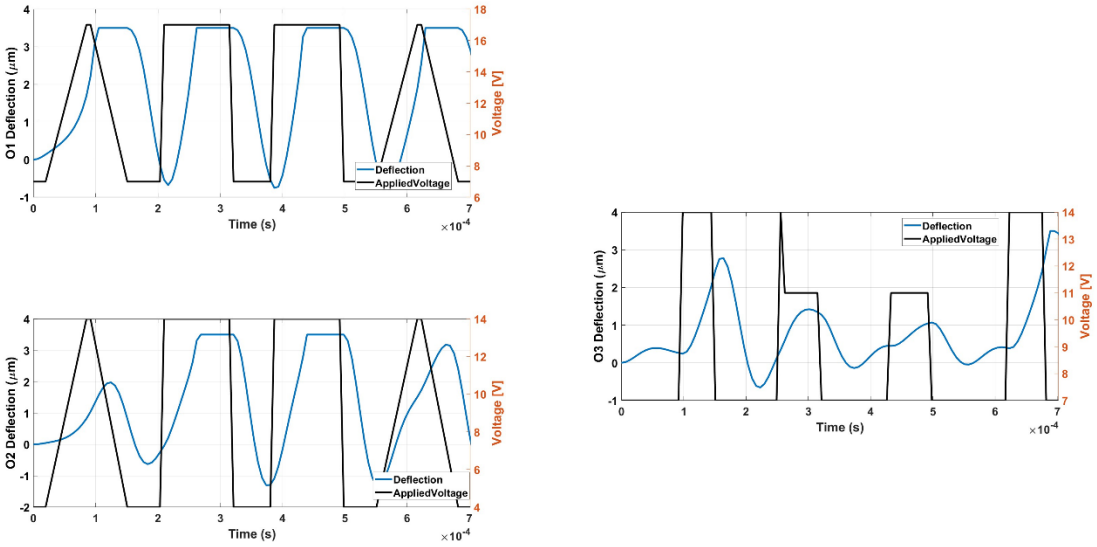

Figure 5.9: MEMS network response with 5600 Hz frequency. (The output MEMS fail to successfully pull-in and classify the input signal.)

The CL900 design natural frequency is around 10 kHz. The figures show a solid classification is expected up to an input frequency below 2.5 kHz. While the second MEMS start to fail in reaching the pull-in, the classification still works for the output MEMS in the range between 2.5 kHz to 5.5 kHz. Finally, starting from 5.6 kHz frequency the network failed to classify the signals. Based on the simulation results, in conclusion, the input signal frequency may not exceed 10-20% of the natural frequency of the MEMS design.

5.3.3 Capillary Sticking Force

Our analysis revealed that the capillary sticking force exerted a noticeable influence on the classification performance of the MEMS network. Higher capillary sticking forces

introduced deviations in classification accuracy. This is true because if the beam stuck the classification task will fail at all. This observation emphasizes the importance of carefully considering and optimizing the capillary sticking force to ensure optimal performance of the MEMS network in signal classification tasks. We may start our claim by assuming that there is a water moisture with a maximum height of the stopper, which can lead to a stiction if there was a contact between the beam and the water, Assuming the worst-case scenario of the contact angle ($\theta = 0°$), we need to estimate the water contact area, we defined a ratio for the contacted area between the beam when contacted the stopper and water to the total length of the beam as shown in Figure 5.10.

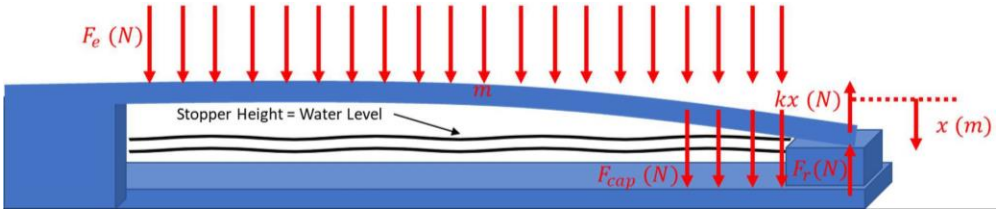

Figure 5.10: Cantilever beam with a capillary force assumed depending on the contact area ratio.

The simulation results for three different cases with a contact ratio of 0.0002,0.00025 and 0.00027 respectively are shown below.

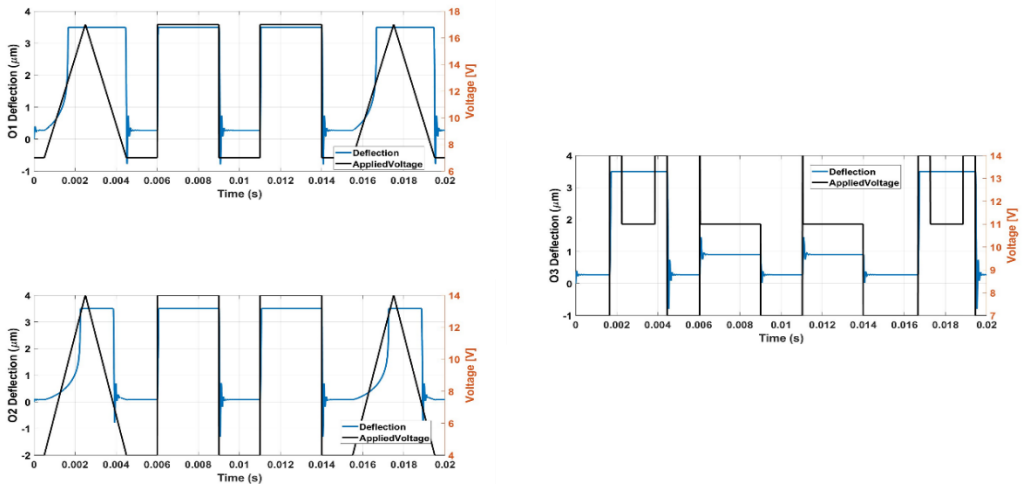

Figure 5.11: MEMS network response in the present of a capillary force with a contact ratio of 0.0002.

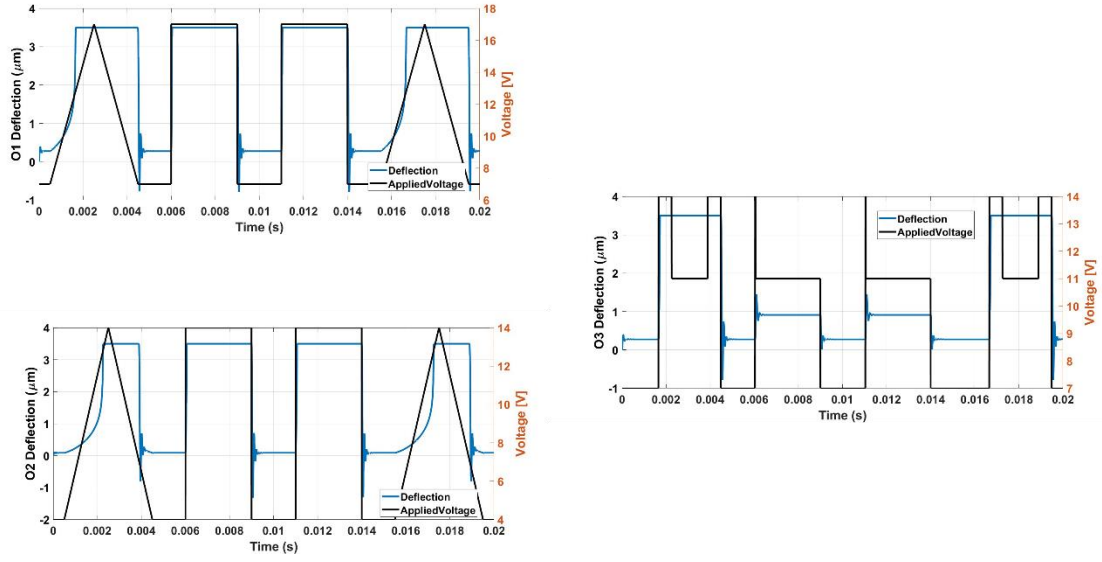

Figure 5.12: MEMS network response in the present of a capillary force with a contact ratio of 0.00025.

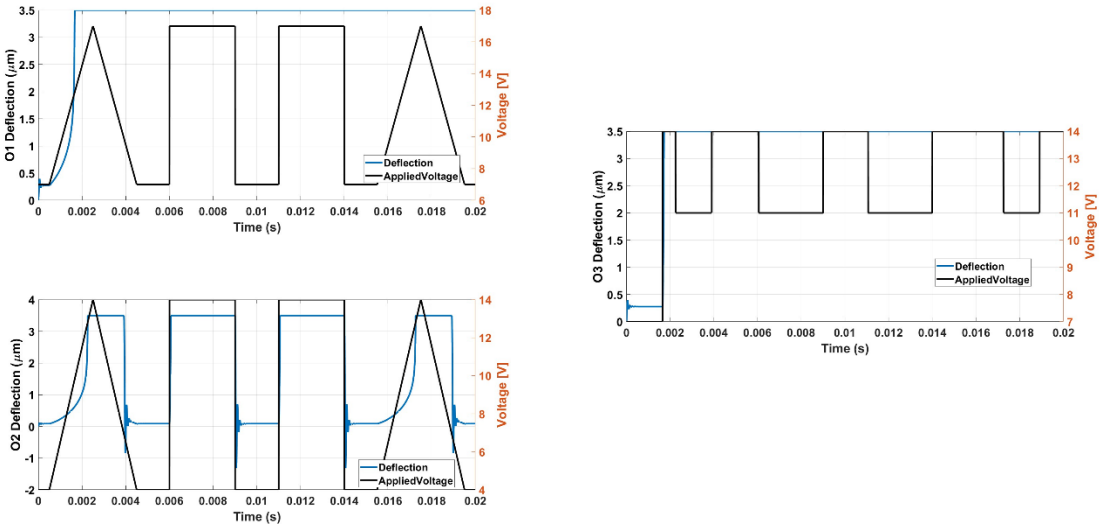

Figure 5.13: MEMS network response in the present of a capillary force with a contact ratio of 0.00028.

We found that the capillary force can be a major parameter that can have the MEMS permanently stick (failure), consequently fail the classification task. We need to be aware of it because increasing the contact area between the beam, the stopper and the water can generate a big force to a point where the restoring force will not be enough to release the beam leading to a permanent beam sticking (device failure). And the whole classification will fail.

CHAPTER 6

THESIS SUMMARY AND FUTURE WORK

6.1 Thesis Summary and Conclusions

The purpose of this thesis was to investigate the possibility of using a MEMS network as a processing unit for the purpose of distinguishing between triangular and square waveforms. The goal of this research was to overcome the constraints of conventional methods of digital signal processing by capitalizing on the benefits of analog computing, more especially by making use of MEMS devices. This study aimed to investigate the feasibility and effectiveness of computing that is based on MEMS, develop a suitable circuit architecture, optimize network parameters, address concerns regarding scalability, and demonstrate the potential of MEMS networks for waveform classification.

It has been proved via simulation and some initial experimentation that a MEMS network is capable of effectively classifying triangle and square waveforms, even when the amplitudes of the two waveforms are the same. The network was able to perform good classification. The designed circuit architecture was able to successfully integrate MEMS devices, capitalizing on the analog computation capabilities of these devices and making use of hysteresis to improve classification performance.

As a result MEMS devices are flexibility to scale, have enabled the integration of numerous computer units, which in turn has made it possible to execute difficult waveform categorization jobs.

In conclusion, the findings of this research were able to successfully illustrate the efficiency as well as the possibility of utilizing a MEMS network as a processing unit for the categorization of triangle and square waveforms. Utilizing the one-of-a-kind characteristics of MEMS devices allowed for the advantages of analog computing to be tapped into. Some of these advantages include low power consumption, real-time processing, and compactness. The findings of this research provide a foundation for the development of efficient and compact systems for real-time waveform analysis and recognition. These contributions to the improvement of waveform classification techniques were made possible by the findings of this research, The goals of this research were not only accomplished, but it also shed light on the enormous potential offered by analog computing that is based on MEMS. The power of analog computing paradigms to overcome the constraints of traditional digital techniques was demonstrated by the successful implementation of the suggested MEMS network as a computing unit for waveform classification.

6.2 Future Work

In the future work, several options will be explored to further enhance the performance of the MEMS-based computing units for waveform classification. One crucial aspect is the

optimization of the MEMS device design to achieve better capacitance changes which are related to the deflection, thereby improving the classification accuracy.

During the initial fabrication process, cantilever beam designs were manufactured, but it was observed that the classification task did not work as expected results. The capacitance change in response to the waveform inputs was relatively low, affecting the ability of the MEMS network to distinguish between triangle and square waveforms accurately, Figure 6.1 shows the cantilever design under the microscope.

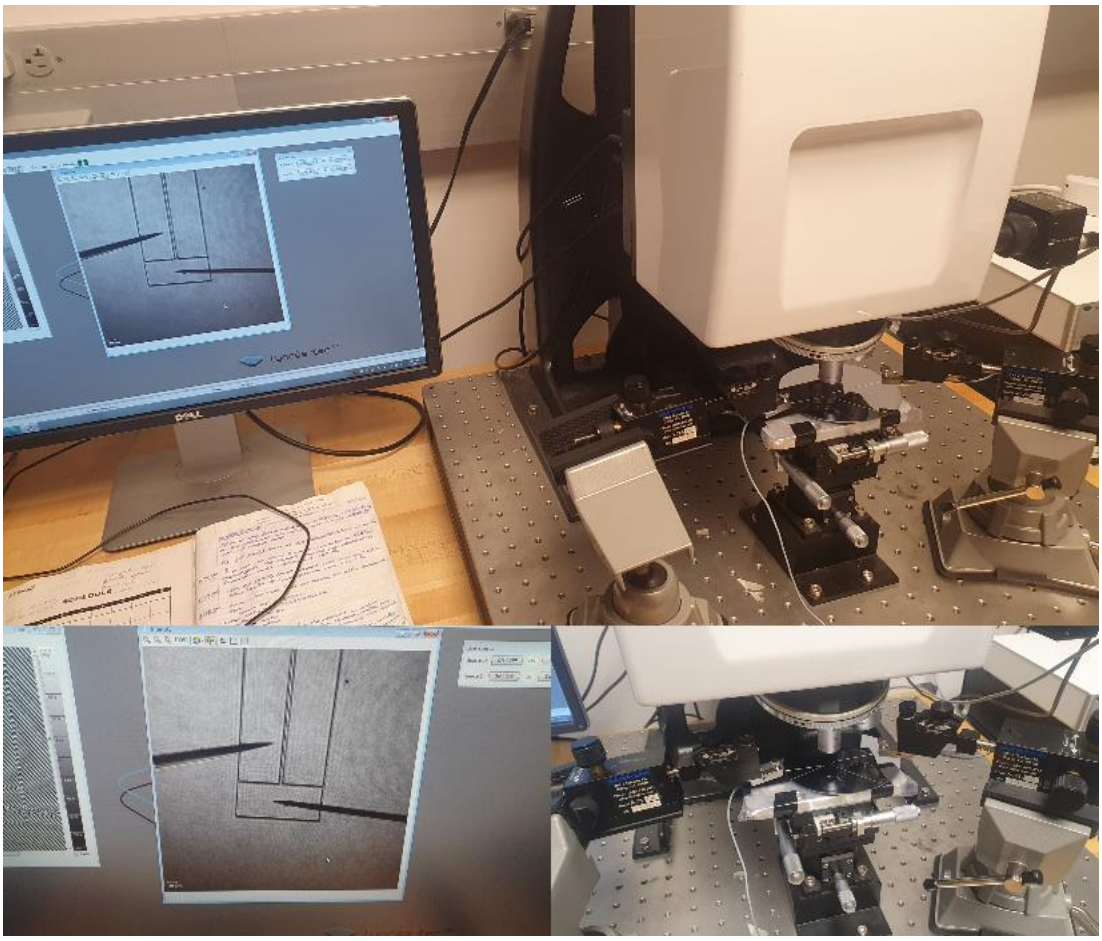

Figure 6.1: CL900 design under microscope.

To address this issue, a clamp-clamp beam design was subsequently fabricated and tested. The clamp-clamp design exhibited a higher capacitance value compared to the cantilever beam, resulting in a more significant response to the waveform inputs.

As a result, the classification task using the clamp-clamp design demonstrated improved accuracy, successfully distinguishing between triangle and square waveforms As shown in Figure 6.2.

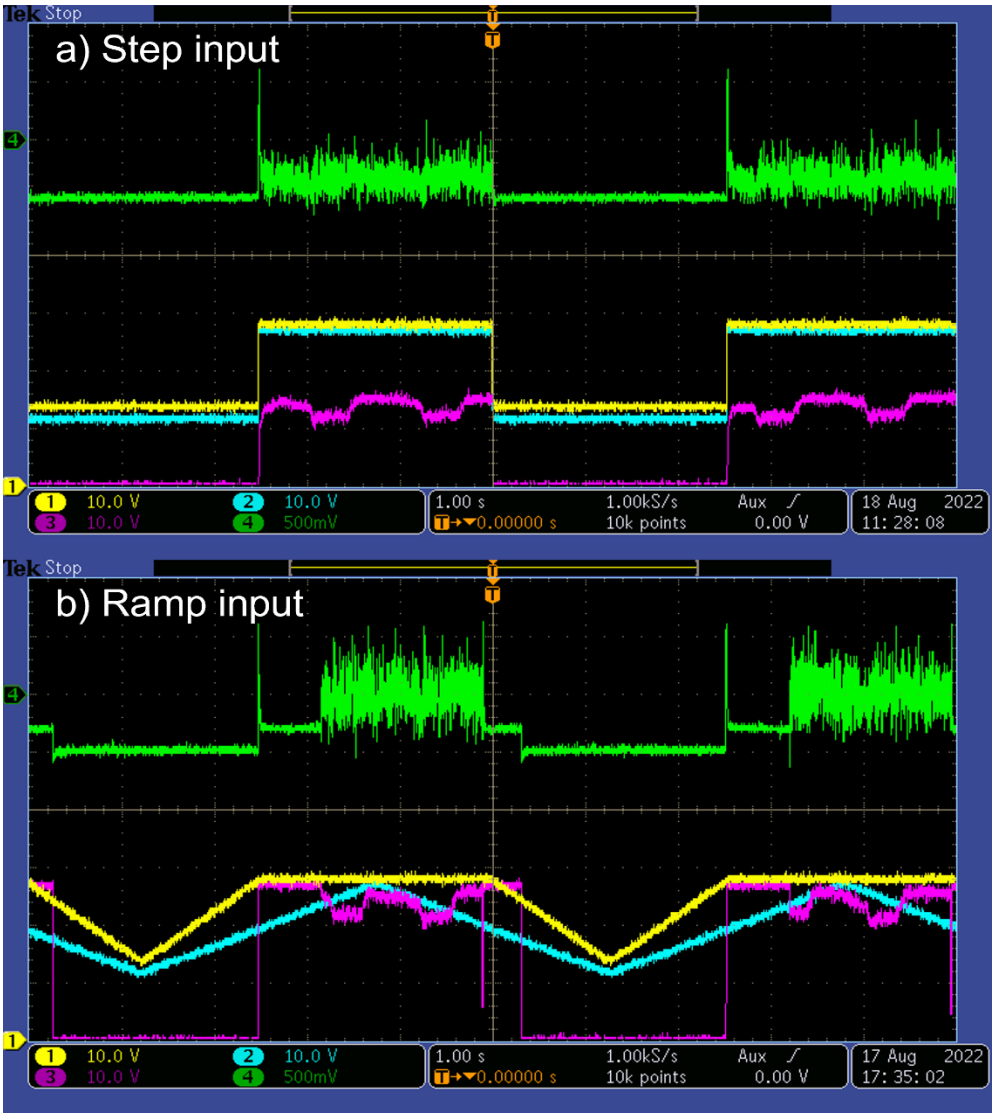

Figure 6.2: Classification Task Experiment Result using Clamped-Clamped Design.

Both square and triangle cases were experimentally tested. When the input signal is square, as shown with both blue and yellow lines, there is no pull-in behavior for the output MEMS as shown with the green line, just a noise. While for the triangle case as shown with the blue and yellow lines, the yellow line is also a triangle but because the oscilloscope is clipping the signal, the output MEMS reach the pull-in, and when the triangle signal is decreasing the output MEMS releases.

In the future work, further refinements will be made to the clamp-clamp design to optimize its performance and ensure robust and consistent capacitance changes.

Lastly, real-world applications for the MEMS-based computing units will be explored. This includes investigating the potential for integrating the MEMS networks into portable and low-power electronic devices for real-time waveform classification in various fields, such as signal processing, communication systems, and wearable technologies.

By focusing on these future directions, this research seeks to contribute to the advancement of analog computing using MEMS and to explore the full capabilities of MEMS networks as powerful computing units for waveform classification tasks, opening up new avenues for innovative applications in diverse technological domains.

References

1. Ejeian, F., Azadi, S., Razmjou, A., Orooji, Y., Kottapalli, A., Warkiani, M. E., & Asadnia, M. (2019). Design and applications of MEMS flow sensors: A review. Sensors and Actuators A: Physical, 295, 483-502.
2. Kainz, A., Steiner, H., Schalko, J., Jachimowicz, A., Kohl, F., Stifter, M., ... & Hortschitz, W. (2018). Distortion-free measurement of electric field strength with a MEMS sensor. Nature electronics, 1(1), 68-73.
3. Chao, Z., Pu, F., Yin, Y., Han, B., & Chen, X. (2018). Research on real-time local rainfall prediction based on MEMS sensors. Journal of Sensors, 2018.
4. Ghazali, F. A. M., Hasan, M. N., Rehman, T., Nafea, M., Ali, M. S. M., & Takahata, K. (2020). MEMS actuators for biomedical applications: a review. Journal of Micromechanics and Microengineering, 30(7), 073001.
5. Yunas, J., Mulyanti, B., Hamidah, I., Mohd Said, M., Pawinanto, R. E., Wan Ali, W. A. F., ... & Yeop Majlis, B. (2020). Polymer-based MEMS electromagnetic actuator for biomedical application: a review. Polymers, 12(5), 1184.
6. Xu, R., & Lin, Y. S. (2021). Flexible and controllable metadevice using self-assembly MEMS actuator. Nano Letters, 21(7), 3205-3210.
7. Tian, W., Li, P., & Yuan, L. (2018). Research and analysis of MEMS switches in different frequency bands. Micromachines, 9(4), 185.
8. Qu, M., Chen, X., Yang, D., Li, D., Zhu, K., Guo, X., & Xie, J. (2021). Monitoring of physiological sounds with wearable device based on piezoelectric MEMS

acoustic sensor. Journal Of Micromechanics and Microengineering, 32(1), 014001.

9. Kaisti, M., Panula, T., Leppänen, J., Punkkinen, R., Jafari Tadi, M., Vasankari, T., ... & Pänkäälä, M. (2019). Clinical assessment of a non-invasive wearable MEMS pressure sensor array for monitoring of arterial pulse waveform, heart rate and detection of atrial fibrillation. NPJ digital medicine, 2(1), 1-10.
10. Wang, Q., Ruan, T., Xu, Q., Yang, B., & Liu, J. (2021). Wearable multifunctional piezoelectric MEMS device for motion monitoring, health warning, and earphone. Nano Energy, 89, 106324.
11. Alsaleem, F. M., Hasan, M. H., & Tesfay, M. K. (2018). A MEMS nonlinear dynamic approach for neural computing. Journal of Microelectromechanical Systems, 27(5), 780-789.
12. Fujii, K., & Nakajima, K. (2017). Harnessing disordered-ensemble quantum dynamics for machine learning. Physical Review Applied, 8(2), 024030.
13. Nakajima, K., Fujii, K., Negoro, M., Mitarai, K., & Kitagawa, M. (2019). Boosting computational power through spatial multiplexing in quantum reservoir computing. Physical Review Applied, 11(3), 034021.
14. Kumar, V., Jafari, R., & Pourkamali, S. (2016). Ultra-low power digitally operated tunable MEMS accelerometer. IEEE Sensors Journal, 16(24), 8715-8721.
15. Zhou, Q., Sussman, A., Chang, J., Dong, J., Zettl, A., & Mickelson, W. (2015). Fast response integrated MEMS microheaters for ultra low power gas detection. Sensors and Actuators A: Physical, 223, 67-75.

16. Ahmed, M., Xu, W., Mohamad, S., Boussaid, F., Lee, Y. K., & Bermak, A. (2019). Fully integrated bidirectional CMOS-MEMS flow sensor with low power pulse operation. IEEE Sensors Journal, 19(9), 3415-3424.
17. Hoppensteadt, F.C. and Izhikevich, E.M., 2001. Synchronization of MEMS resonators and mechanical neurocomputing. IEEE Transactions on Circuits and Systems I: Fundamental Theory and Applications, 48(2), pp.133-138.
18. Zheng, T., Yang, W., Sun, J., Xiong, X., Wang, Z., Li, Z., & Zou, X. (2021). Enhancing performance of reservoir computing system based on coupled MEMS resonators. Sensors, 21(9), 2961.
19. Kumar, A. and Mohanty, P., 2017. Autoassociative memory and pattern recognition in micromechanical oscillator network. Scientific reports, 7(1), p.411.
20. Alsaleem, F.M., Hasan, M.H. and Tesfay, M.K., 2018. A MEMS nonlinear dynamic approach for neural computing. Journal of Microelectromechanical Systems, 27(5), pp.780-789.
21. Emad-Ud-Din, M., Hasan, M.H., Jafari, R., Pourkamali, S. and Alsaleem, F., 2021. Simulation for a Mems-Based CTRNN Ultra-Low Power Implementation of Human Activity Recognition. Frontiers in Digital Health, 3, p.731076.
22. Nikfarjam, H., Megdadi, M., Okour, M., Pourkamali, S. and Alsaleem, F., 2023. Theoretical and Experimental Investigation of Using Multi-Degree of Freedom Electrostatically Actuated Micro-Structures in Performing Classification Problems. IEEE Sensors Journal.

23. Lukoševičius, M., Jaeger, H. and Schrauwen, B., 2012. Reservoir computing trends. KI-Künstliche Intelligenz, 26, pp.365-371.
24. Paquot, Y., Duport, F., Smerieri, A., Dambre, J., Schrauwen, B., Haelterman, M. and Massar, S., 2012. Optoelectronic reservoir computing. Scientific reports, 2(1), p.287.
25. Tanaka, G., Yamane, T., Héroux, J. B., Nakane, R., Kanazawa, N., Takeda, S., ... & Hirose, A. (2019). Recent advances in physical reservoir computing: A review. Neural Networks, 115, 100-123.
26. Lukoševičius, M., & Jaeger, H. (2009). Reservoir computing approaches to recurrent neural network training. Computer Science Review, 3(3), 127-149.
27. Hinaut, X., & Dominey, P. F. (2013). Real-time parallel processing of grammatical structure in the fronto-striatal system: A recurrent network simulation study using reservoir computing. PloS one, 8(2), e52946.
28. Nakada, K., Suzuki, S., Suzuki, E., Terasaki, Y., Asai, T., & Sasaki, T. (2022). An information theoretic parameter tuning for MEMS-based reservoir computing. Nonlinear Theory and Its Applications, IEICE, 13(2), 459-464.
29. Barazani, B., Dion, G., Morissette, J. F., Beaudoin, L., & Sylvestre, J. (2020). Microfabricated neuroaccelerometer: integrating sensing and reservoir computing in MEMS. Journal of Microelectromechanical Systems, 29(3), 338-347.
30. Younis, M.I., 2011. MEMS linear and nonlinear statics and dynamics (Vol. 20). Springer Science & Business Media.

31. H Hasan, M., Al-Ramini, A., Abdel-Rahman, E., Jafari, R. and Alsaleem, F., 2020. Colocalized sensing and intelligent computing in micro-sensors. Sensors, 20(21), p.6346.
32. H Hasan, M., Abbasalipour, A., Nikfarjam, H., Pourkamali, S., Emad-Ud-Din, M., Jafari, R. and Alsaleem, F., 2021. Exploiting pull-in/pull-out hysteresis in electrostatic MEMS sensor networks to realize a novel sensing continuous-time recurrent neural network. Micromachines, 12(3), p.268.
33. Mizumoto, T., Hirai, Y., Banerjee, A. and Tsuchiya, T., 2022, January. MEMS Reservoir Computing using Frequency Modulated Accelerometer. In 2022 IEEE 35th International Conference on Micro Electro Mechanical Systems Conference (MEMS) (pp. 487-490). IEEE.
34. Pallay, M., Miles, R.N. and Towfighian, S., 2019. A tunable electrostatic MEMS pressure switch. IEEE Transactions on Industrial Electronics, 67(11), pp.9833-9840.
35. Lee, M., Li, H., Birla, M.B., Li, G., Wang, T.D. and Oldham, K.R., 2022. Capacitive Sensing for 2-D Electrostatic MEMS Scanner in a Clinical Endomicroscope. IEEE Sensors Journal, 22(24), pp.24493-24503.
36. Daeichin, M., Miles, R. and Towfighian, S., 2020. Lateral pull-in instability of electrostatic MEMS transducers employing repulsive force. Nonlinear Dynamics, 100, pp.1927-1940.

37. Liu, X., Zhang, L. and Zhang, M., 2022. Studies on Pull-in instability of an electrostatic MEMS actuator: dynamical system approach. J. Appl. Anal. Comput, 12, pp.850-861.

APPENDIX A

Appendix A shows more investigation for the different case studies that we show through this work with more simulation results.

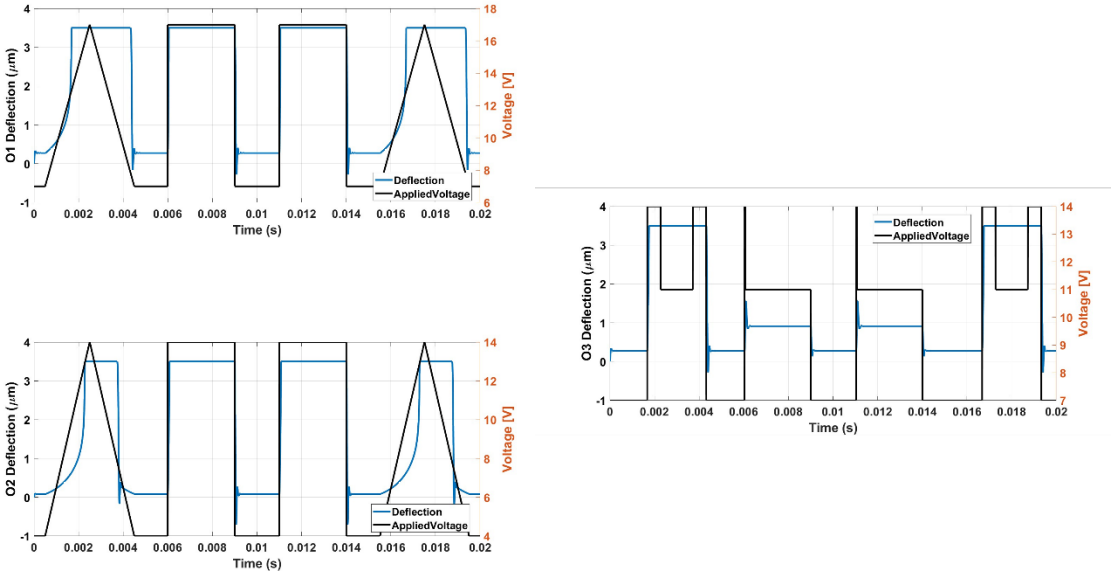

Figure A.1: MEMS network response with ζ=0.4

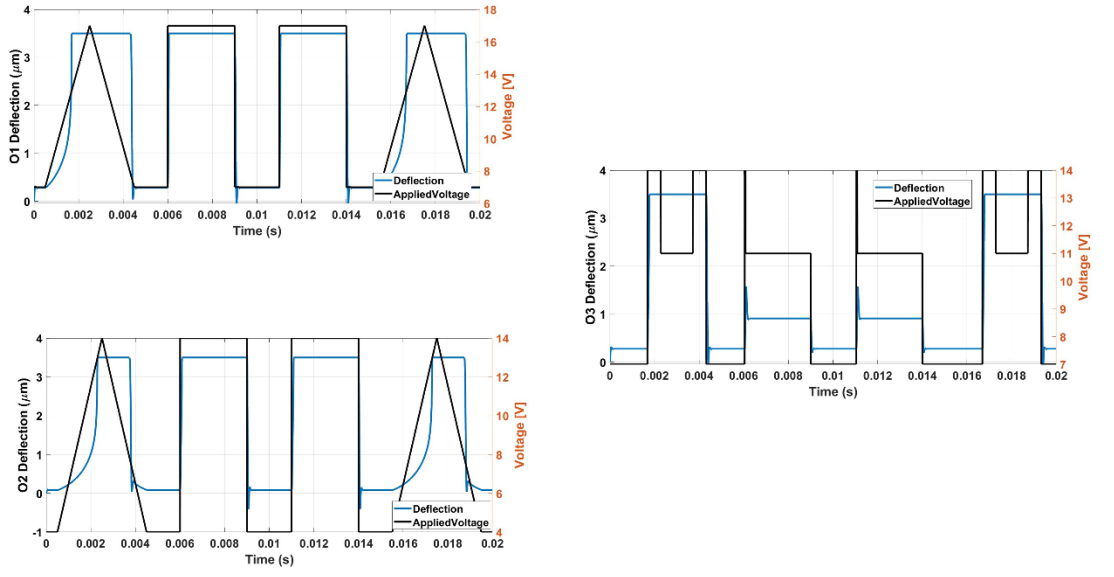

Figure A.2: MEMS network response with ζ=0.5

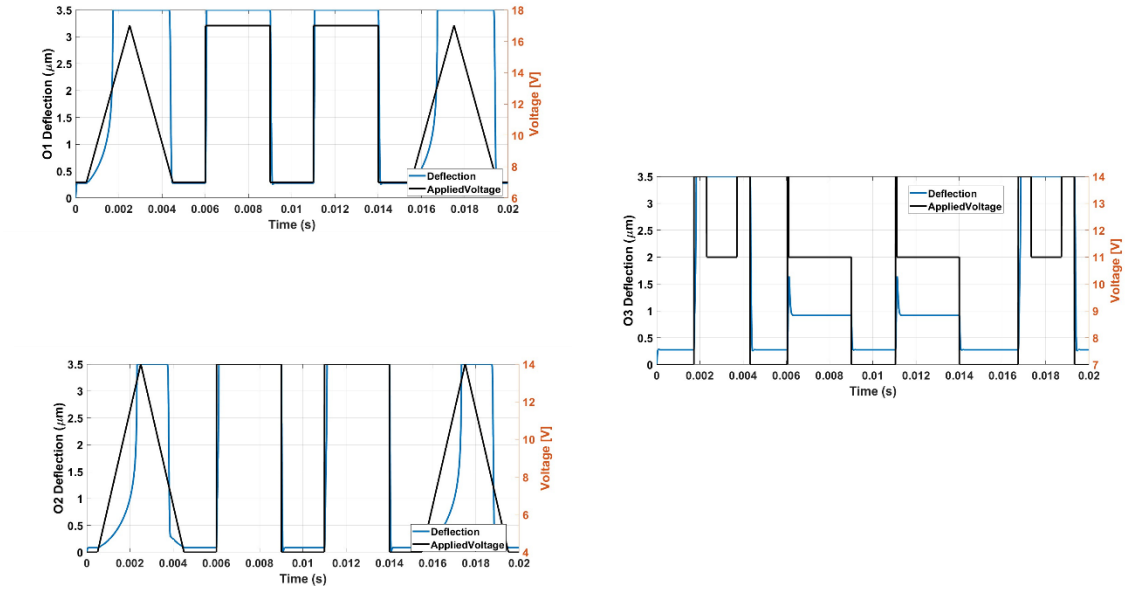

Figure A.3: MEMS network response with ζ=0.75

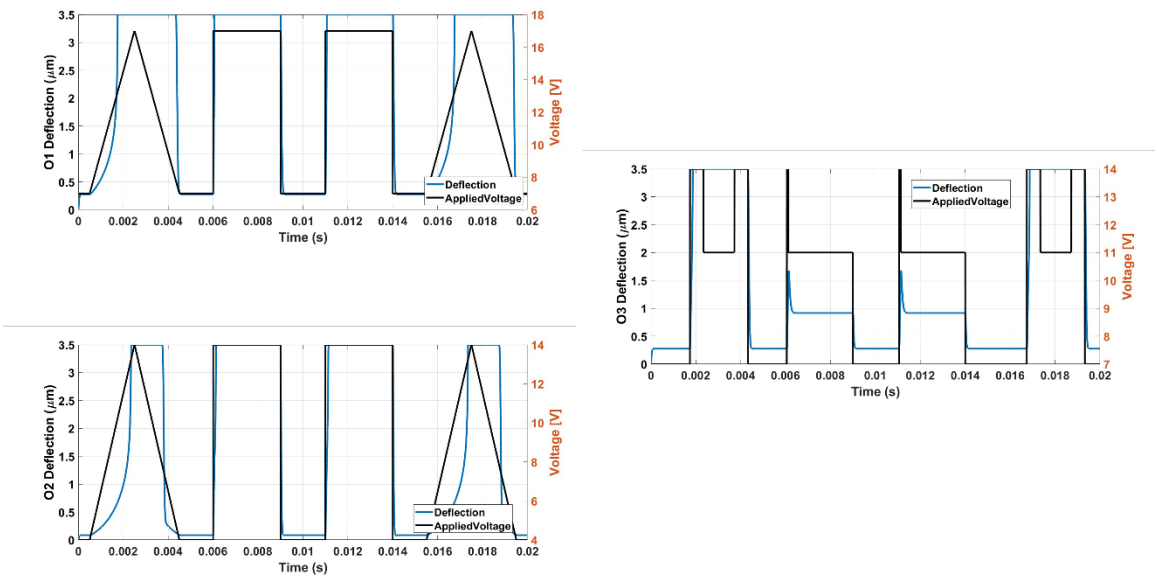

Figure A.4: MEMS network response with ζ=0.9

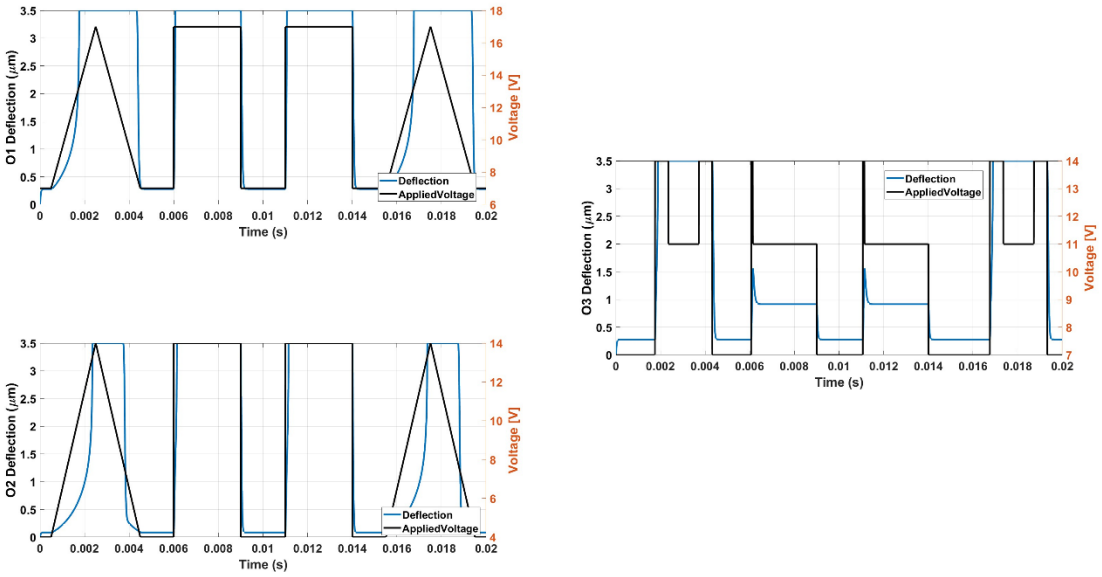

Figure A.5: MEMS network response with ζ=1

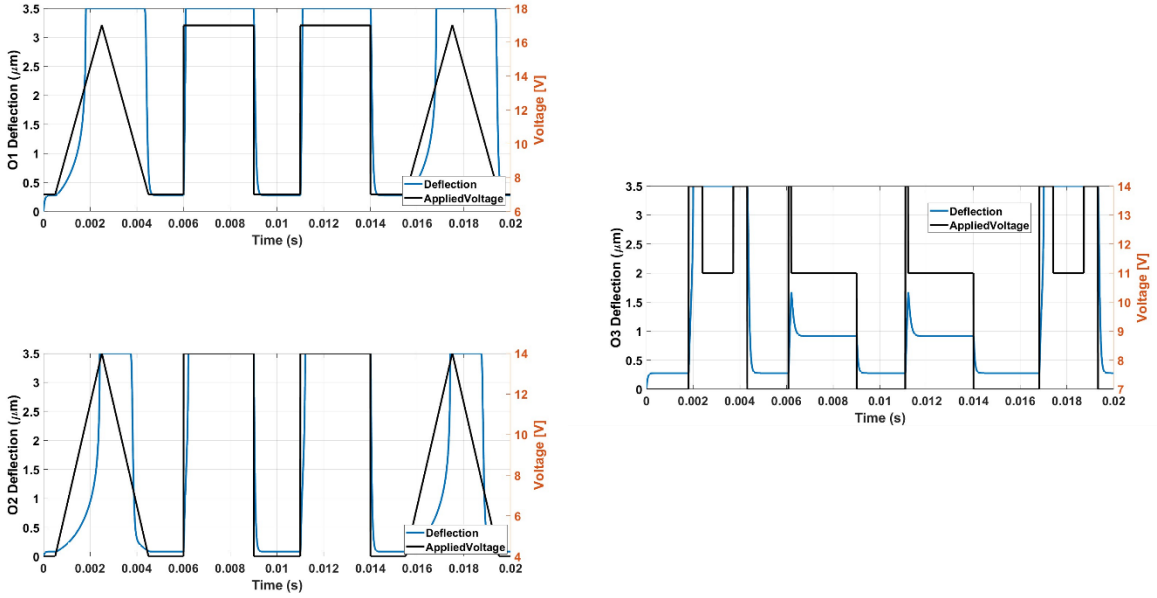

Figure A.6: MEMS network response with ζ=1.5

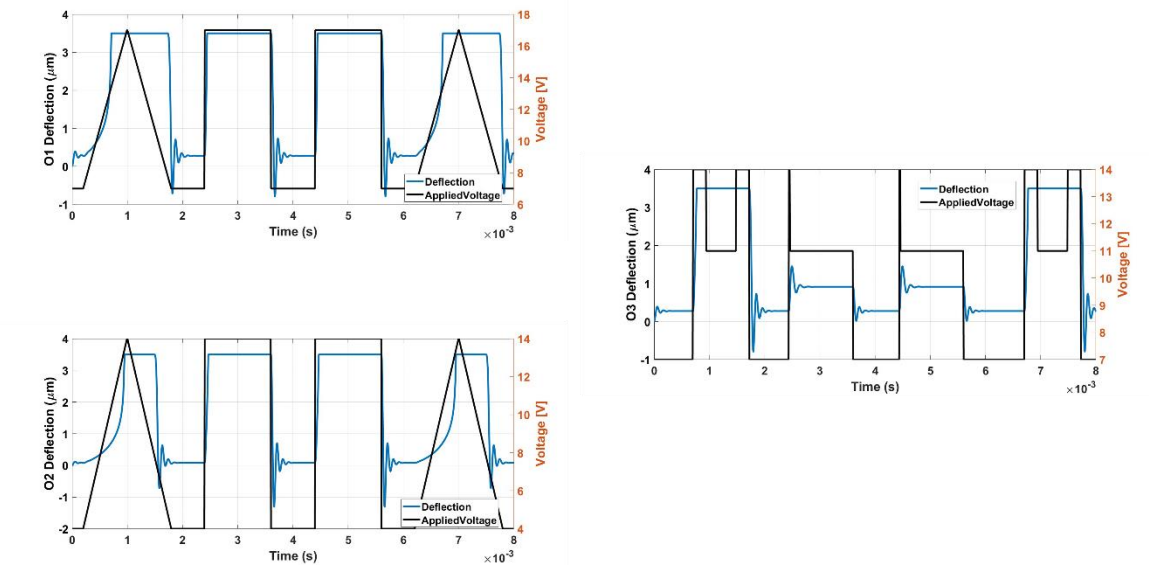

Figure A.7: MEMS network response with 500 Hz frequency.

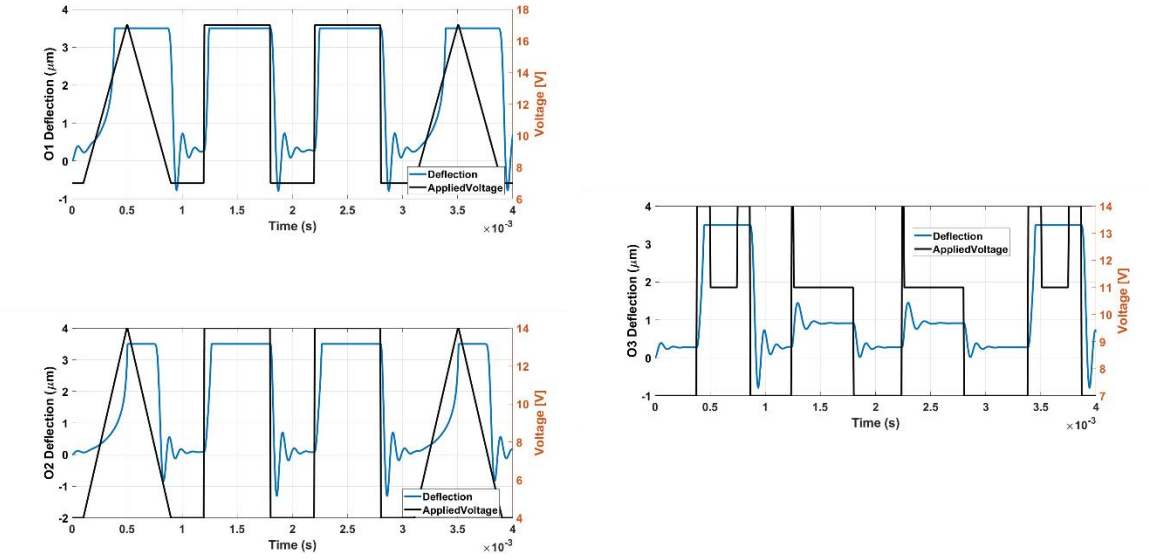

Figure A.8: MEMS network response with 1000 Hz frequency.

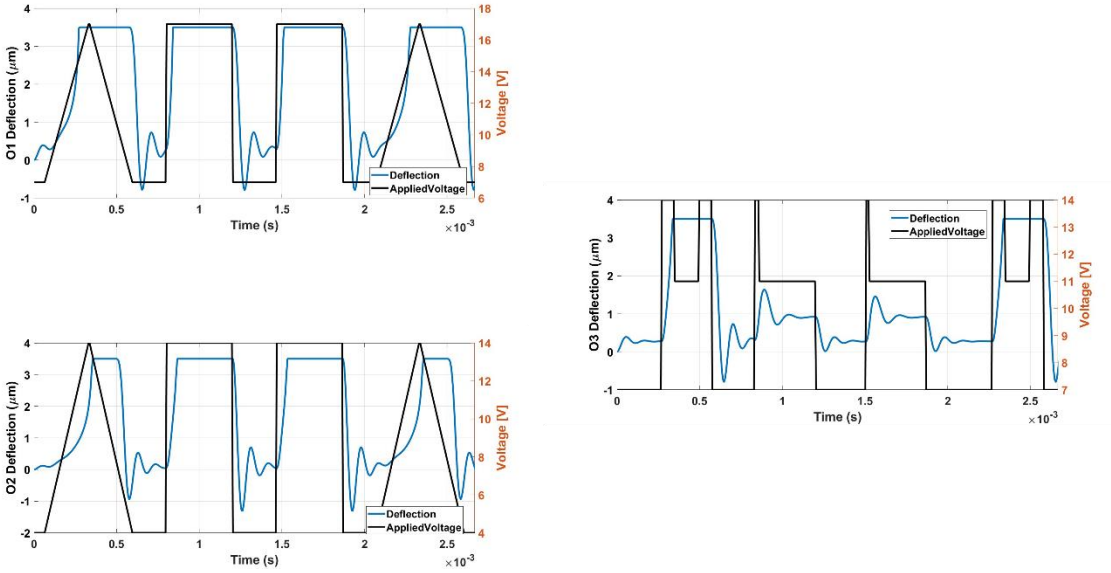

Figure A.9: MEMS network response with 1500 Hz frequency.

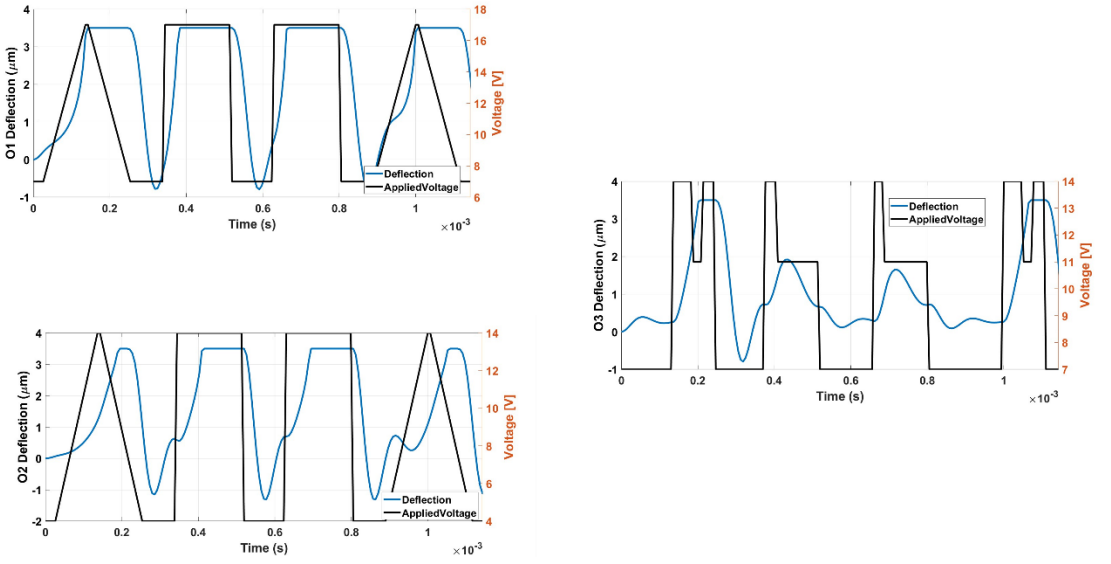

Figure A.10: MEMS network response with 3500 Hz frequency.

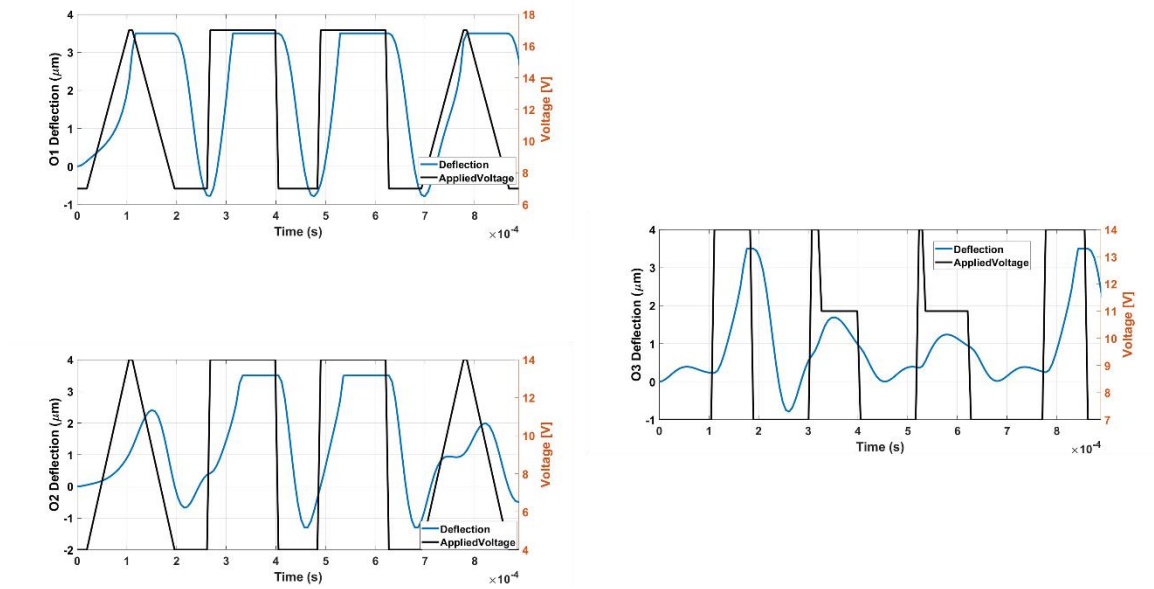

Figure A.11: MEMS network response with 4500 Hz frequency.